1 A time series analysis of transparent exopolymer particle distributions and C:N
2 stoichiometry in the subtropical North Pacific: a key process in net community
3 production and preformed nitrate anomalies?

5 Kieran Curran[1], Tracy A. Villareal[2], Robert T. Letscher[1,3]

6   1   Ocean Process Analysis Laboratory, University of New Hampshire, Durham, NH, 03824 USA
7   2   Marine Science Institute, University of Texas at Austin, Port Aransas, TX 78373 USA
8   3   Department of Earth Sciences, University of New Hampshire, Durham, NH 03824 USA

9 *Correspondence to*: Robert T. Letscher (robert.letscher@unh.edu)

Abstract

11 Within the oligotrophic subtropical oceans, summertime dissolved inorganic carbon drawdown despite
12 nutrient limitation in surface waters and subsurface oxygen consumption in the absence of Redfieldian
13 stoichiometric nitrate release are two phenomena still awaiting a full mechanistic characterization. Many
14 processes may contribute to these anomalies including N_2 fixation, non-Redfieldian DOM cycling, vertically
15 migrating phytoplankton, heterotrophic NO_3^- uptake and vertical NO_3^- injection events. While these
16 processes have been measured or modelled they generally cannot fully account for the magnitudes of
17 oxygen/nitrate anomalies and excess dissolved inorganic drawdown observed in many oligotrophic
18 subtropical waters. One other candidate process that may contribute to both phenomena is the formation
19 of carbon-rich transparent exopolymer particles (TEP) and Coomassie-stainable particles (CSP) from
20 dissolved organic precursors in surface waters and their subsequent export and remineralization below,
21 however, few TEP and CSP data exist from the oligotrophic ocean. Here we present a multi-year time-
22 series (Jan 2020 – Sep 2022) analysis of TEP, CSP and total dissolved carbohydrate concentrations at both
23 Station ALOHA (22°45',158 °W) and along a meridional transect during June 2021 from 22°45' to 31°N
24 within the North Pacific subtropical gyre. Exopolymer C:N stoichiometry at Station ALOHA varied between
25 16.4 – 34.3, with values being more carbon-rich in summer (26-34); ratios were higher (33-38) toward the
26 gyre centre at 31°N. TEP concentrations were consistently elevated in surface waters through Spring-
27 Autumn (4-8 μM C after carbon conversion) at Station ALOHA with lower concentrations (~1.5-3 μM C)
28 and more uniform vertical distribution during winter, indicating that TEP accumulated in surface waters
29 may vertically sink and be exported with winter mixing. The accumulation of exopolymers in surface
30 waters through Spring-Autumn and its subsequent vertical export may account for 6.5-20% of net
31 community production, helping to reduce the estimated imbalance of N supply and demand at this site to
32 <10%. The upper ocean exopolymer cycle may explain 22-67% of the observed oxygen/nitrate anomalies,
33 helping to close the C, N, and O_2 budgets at station ALOHA, while leaving room for significant contributions
34 from other processes such as vertically migrating phytoplankton and heterotrophic nitrate uptake. These
35 results suggest that exopolymer production and cycling may be more important to open ocean carbon
36 biogeochemistry and the biological pump than previously expected.

37

1 Introduction

Subtropical oceans constitute one of earth's largest biomes, where the euphotic water column exhibits sustained macronutrient limitation due to strong thermal stratification (Reygondeau et al., 2013). Consistently low euphotic zone chlorophyll concentrations observed in these regions lead to depressed primary production estimates using ocean-colour satellite and bio-optical float profile data (Longhurst et al., 1995; Long et al., 2021; Westberry et al., 2023). Despite this assumption of low productivity, various measured rates of annual net community production (NCP) and total annual carbon export from the ocean subtropics suggest a biological pump strength that is maintained at levels consistent with mesotrophic oceanic regions receiving a higher vertical nutrient injection flux (Gruber et al., 1998; Emerson, 2014; Teng et al., 2014; Roshan and DeVries, 2017; Quay et al., 2020; Karl et al., 2021; Quay and Stephens, 2025).

Moderate rates of summertime surface dissolved inorganic carbon (DIC) drawdown are observed in low-chlorophyll Atlantic and Pacific subtropical oceans (2-3 mol C m^{-2} y^{-1}) despite limiting nitrate and phosphate concentrations, and stratification that would seem to limit diapycnal supply of nutrients to the euphotic zone for most of the year (Sambrotto et al., 1993; Michaels et al., 1994; Dave and Lozier, 2010; Williams et al., 2013; Emerson, 2014). Processes of nutrient enrichment such as N_2 fixation, episodic mixing events, and iron-rich dust deposition are unable to fully provide sufficient nutrient supply to sustain this persistent summertime anomaly (Johnson et al., 2010; Chow et al., 2017; Fawcett et al., 2018; Letscher and Villareal, 2018; Letelier et al., 2019; Karl et al., 2021). In addition, most subtropical regions exhibit subsurface respiration without concomitant nitrate release expected from the remineralization of Redfieldian organic matter. This produces a widespread negative preformed nitrate (preNO$_3^-$) anomaly between ~120-180m (Emerson and Hayward, 1995; Abell et al., 2005; Ascani et al., 2013; Letscher and Villareal, 2018; Smyth and Letscher, 2023), and stoichiometrically balanced positive preNO$_3^-$ anomalies found within the upper 100m where O_2 is produced without stoichiometric NO$_3^-$ drawdown (Letscher and Villareal, 2018). The introduction of allochthonous macronutrient supply to the surface mixed layer by vertically migrating phytoplankton or the production and export of non-Redfieldian organic matter (high elemental carbon:nitrogen ratio) are two potential processes which may couple these three phenomena and help explain the elevated surface DIC drawdown and positive preNO$_3^-$ as well as negative preNO$_3^-$ below the sub-surface chlorophyll maximum in these regions (Letscher and Villareal, 2018) .

Transparent exopolymer particles (TEP), mostly comprised of acidic polysaccharides, are ubiquitous throughout the oceans, where they tend to accumulate in surface waters due to their low density (Azetsu-Scott and Passow, 2004). Exopolymers are typically observed as being carbon-rich, with C:N ratios of >20:1 (Mari et al., 2001; Engel and Passow, 2001; Passow, 2002b; Guo et al., 2022), which makes them a candidate for surface mixed layer DIC drawdown with minimal nitrogen requirement, particularly if composed of pure carbohydrate (e.g. 1 C : 1 O_2 : 0 N). While most abundant during large blooms of phytoplankton in eutrophic waters, TEP and their precursors are produced by a wide variety of phytoplankton and bacteria across different marine and aquatic environments (Passow et al., 1994; Nosaka et al., 2017; Zamanillo et al., 2019). Exopolymers act as a bridge between the dissolved and particulate fractions of marine organic matter, with dynamic assembly and disassembly of marine gels helping to fill the size continuum of particles in the ocean (Verdugo et al., 2004; Verdugo, 2012). The related but distinct Coomassie stainable particles (CSP) are thought to track the more protein-rich component of the marine exopolymer/gel pool, which likely impacts the fate of these particles differently

80   than the polysaccharide-rich TEP pool (Cisternas-Novoa et al., 2015; Zamanillo et al., 2021). TEP
81   contributes to sinking exopolymer aggregates, which in turn constitute a significant flux of POC to the
82   upper mesopelagic zone where much of this organic matter may be consumed by aggregate-associated
83   bacteria (Wurl et al., 2011b; Nagata et al., 2021) and zooplankton (Ling and Alldredge, 2003).

84   TEP production from phytoplankton exudates is associated with excess DIC drawdown even in nutrient-
85   replete water. In these regions, carbon overconsumption can be as high as 30-40% with respect to nitrate
86   and phosphate removal and POM C:N:P stoichiometry (Toggweiler, 1993). Surface mixed layer
87   exopolymer production may increase as cells are stressed by nutrient limitation or photo-oxidative
88   stresses (Berman-Frank et al., 2007; Ortega-Retuerta et al., 2009a; Iuculano et al., 2017), persistent in
89   many subtropical surface waters. Therefore, despite lower phytoplankton biomass in these oligotrophic
90   regions, significant TEP production and seasonal variability may still occur.

91   Given that different oligotrophic regions exhibit significant variability in the elemental stoichiometry of
92   organic matter including biomass (Martiny et al., 2013), detrital POM, and DOM (Letscher and Moore,
93   2015; Liang et al., 2023), across depth and time, region-specific measurements are needed to quantify the
94   importance of exopolymer particles to pelagic biogeochemistry of different regions (McCarthy et al., 1996;
95   Mari et al., 2001; Passow, 2002b; Beauvais et al., 2003).

96   In this study, we assess whether significant depth, temporal, and latitudinal gradients exist in: 1).
97   exopolymer abundance and its associated C:N content that may help to explain the seasonal excess DIC
98   drawdown in the absence of known nutrient supply pathways (e.g. Johnson et al., 2010), and 2)
99   potentially related subsurface $preNO_3^-$ anomalies present within the North Pacific subtropical gyre
100   (NPSG). To do this, we sampled two classes of exopolymers: carbohydrate-rich transparent exopolymer
101   particles (TEP) and protein-containing Coomassie-stainable particles (CSP) as well as dissolved
102   carbohydrates (precursor molecules of larger exopolymer particles (Passow, 2000; Ortega-Retuerta et
103   al., 2009b; Arnosti et al., 2021)), for nearly three years to quantify their concentrations, vertical
104   distributions, and seasonal and latitudinal variability.

105

106   In order to produce quantitative estimates of TEP and CSP concentrations, we also directly estimated the
107   organic C and N content of exopolymers spontaneously assembled under controlled conditions in the field
108   to convert TEP and CSP values to carbon and nitrogen equivalents. With these quantitative estimates of
109   TEP-C and CSP-N concentrations, we then discuss the potential contributions of the exopolymer cycle for
110   explaining surface mixed layer excess DIC drawdown and subsurface $preNO_3^-$ anomalies. This contribution
111   helps to close the C, N, and O_2 budgets at station ALOHA,, and may apply to the carbon and nutrient
112   biogeochemistry of the subtropical oceans more generally.

113

114 2 Methods

115 2.1 Sample collection

116   Water samples for measurements of TEP, CSP, and dissolved polysaccharides were collected using a
117   Niskin rosette onboard the RV *Kilo Moana* from 15 cruises between January 2020 and September 2022.
118   14 cruises were part of the Hawaiian Ocean Time-series (HOT) sampling program at Station ALOHA (22°

119   45' N 158° W), with 1 cruise sampling 10 stations in the North Pacific Gyre along a nominal 158ºW

120   transect from Station ALOHA to 31° N during June 2021, also on RV *Kilo Moana* (Fig. 1). Vertical profiles

121   of salinity (Sea-Bird SBE-09), temperature (Sea-Bird SBE-3 Plus) and oxygen (Sea-Bird SBE-43) were also

122   collected from the rosette CTD instrument package.

123

124
125
126
127
128
129
130
131
132
133
134
135
136
137
138
139
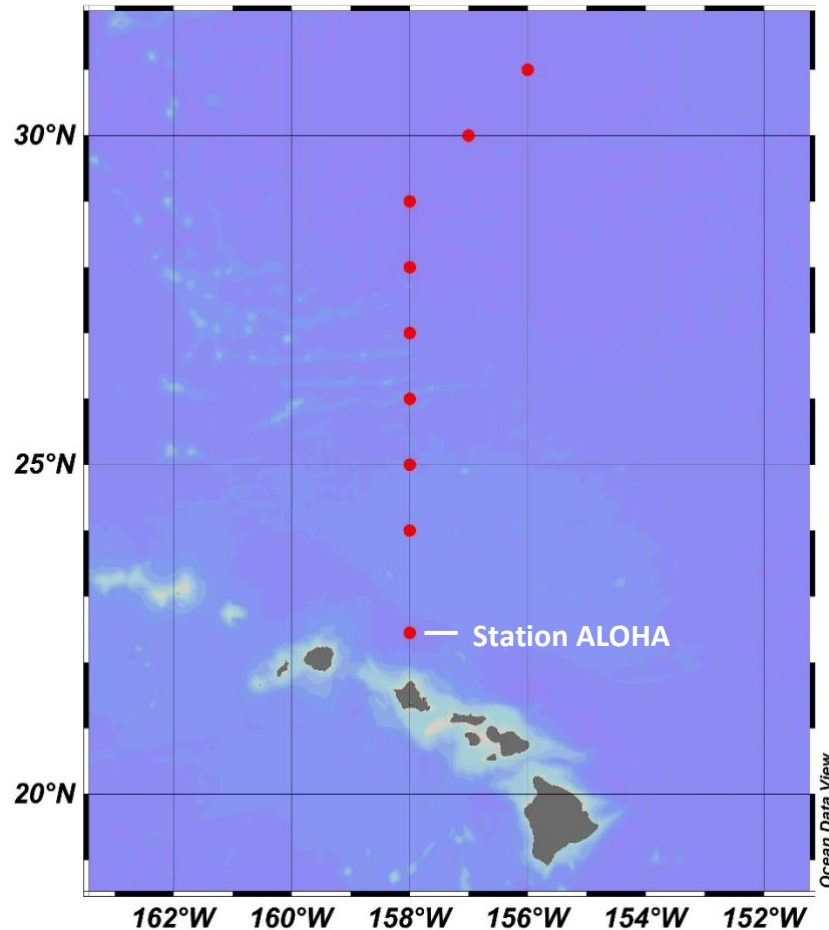
140   Figure 1. Map showing the location of Station ALOHA where time series measurements were collected and the
141   stations along the June 2021 transect between ALOHA and 31°N.

2.2 Quantification of transparent exopolymer particles (TEP) and Coomassie-stainable particles (CSP)

144   Water samples for TEP and CSP (0.5-2.0L) were taken from 5-8 depths and stored in polycarbonate bottles

145   (Corning) in blacked-out carriers until filtration. Samples were processed from deepest to shallowest to

146   minimize any effects of small temperature changes on exopolymer formation dynamics. Water samples

147   for TEP and CSP were filtered using 0.4 μm pore-size, 25mm diameter polycarbonate filters (Whatman)

148   using a peristaltic pump (Cole-Parmer) and silicone tubing (Masterflex). Filters were then placed onto a

149   vacuum filtration rig and dyed with acidified (pH 2.5) 0.02% Alcian Blue (AB) solution (Alcian Blue 8X,

150   Sigma Aldrich) for TEP samples following Bittar et al. (2015) and 0.04% Coomassie brilliant blue (CBB)

151   (SERVA) solution (pH 7.4) for CSP samples following Cisternas-Novoa et al. (2015). Dyed filters were placed

152   in polypropylene vials (Falcon) and frozen at -20ºC, and 2-day shipped back to the shore-based laboratory

in ice-packed coolers (Pelican). TEP samples were extracted in 6 ml 80% sulphuric acid solution for 2 hrs and absorbance read at 787nm. CSP samples were extracted in 4 ml 3% sodium dodecyl sulphate (SDS) in 50% isopropyl alcohol solution for 2 hrs at 37°C under ultrasonication and read at 615nm. Absorbance values were blanked against the same type of polycarbonate filters after filtration of 500ml ultrapure water. Blanks were also taken with 500ml 0.2 µm filtered seawater to check that there was no bias resulting from sub-0.2 µm organic material from seawater retained on the filters. These blanks were not significantly different and had a combined coefficient of variation of 0.039. Absorbance values were calibrated against a dilution series of xanthan gum (XG) (Sigma) and bovine albumin (BA) (Sigma) for TEP and CSP respectively. Concentration units are therefore expressed as µg XG equivalents L^{-1} and µg BA equivalents L^{-1} following the literature convention (e.g., Cisternas-Novoa et al. (2015)) using the spectrophotometric method for TEP and CSP quantification in Figure 2. TEP sample replicates had a mean coefficient of variation of 0.04 µg XG equiv. L^{-1} and CSP samples 0.14 µg BA equiv. L^{-1} (n=24) from 8 sets of triplicate measurements.

2.3 Dissolved carbohydrates
Water samples for dissolved carbohydrate analysis were gravity filtered from the Niskin rosette using a 47mm combusted GF/F filter (Whatman; 0.7µm nominal pore size) into acid cleaned and furnaced glass vials. Vials were frozen at -20ºC and transported similar to above for lab analysis. Using the approach of Myklestad et al (1997), total HCl-hydrolysable carbohydrates (TCHO) were measured against a glucose calibration standard and expressed in µM carbon. The method uses the alkaline ferricyanide reaction with 2,4,6-tripyridyl-*s*-triazine (TPTZ) that produces a deep violet color with reduced iron, allowing sensitive measurement of low carbohydrate concentrations with spectrophotometry. Reagents were made fresh for each run of samples and kept in blacked-out glassware. Coefficients of variation averaged 2.5% on triplicate analyses of dissolved carbohydrate.

2.4 Carbon and Nitrogen conversion factors
During field sampling at station ALOHA (22.75°N, 158°W) and from 31° N, 156°W in June 2021 and October 2021 from station ALOHA alone, 3 x 10 litre volumes of seawater from two depths (5m, 125m) were filtered through a 0.2 µm capsule filter (Pall) into opaque HDPE plastic bottles and stored in the dark while at sea at sample depth temperature ±1°C. Bottles were left for 80-100 hrs to allow sufficient time for exopolymer to spontaneously reform from the dissolved fraction. From these bottles, duplicate filtrations (1.5L) were performed for TEP and CSP concentrations as above and duplicate filtrations for particulate carbon and nitrogen were taken onto 47mm GF filters (Whatman) for CHN analysis of the collected exopolymer particles.

Particulate carbon and nitrogen data (in µM C and µM N) were then used with the measurements of TEP and CSP (in µg XG equiv. L^{-1} and µg BA equiv. L^{-1}) to convert the latter exopolymer concentration units to µM C and µM N using carbon and nitrogen conversion factors (CCF and NCF).

$$CCF = \frac{\mu M\ Particulate\ Carbon}{\mu g\ XG\ equiv\ L^{-1}} \qquad (1)$$

$$NCF = \frac{\mu M\ Particulate\ Nitrogen}{\mu g\ BA\ equiv\ L^{-1}} \qquad (2)$$

191 TEP carbon (TEP-C) and CSP nitrogen (CSP-N) concentrations are thereafter converted and expressed in
192 µM units of carbon and nitrogen respectively.

193

3 Results

3.1 Carbon and Nitrogen conversion factors

196 Table 1. TEP-C and CSP-N conversion factors and exopolymer C:N ratios measured from exopolymer ingrowth
197 incubations of 0.2 µm-filtered seawater conducted in June and October '21 at station ALOHA and at the northern
198 end of the June '21 transect (31°N, 156°W); values in parentheses are coefficients of variation.

Conversions	TEP-C Jun 21	TEP-C Oct 21	CSP-N Jun 21	CSP-N Oct 21	C:N Jun 21	C:N Oct 21
ALOHA 5 m	0.529 (0.02)	0.577 (0.02)	0.018 (0.03)	0.012 (0.18)	25.7 (0.01)	18.54 (0.16)
ALOHA 125 m	0.627 (0.05)	0.600 (0.19)	0.005 (0.23)	0.013 (0.27)	34.3 (0.11)	16.40 (0.36)
31°N 5m	0.656 (0.12)		0.004 (0.05)		33.2 (0.04)	
31°N 125m	0.759 (0.05)		0.003 (0.19)		38.1 (0.01)	

200 Carbon conversion factors for TEP-C at station ALOHA varied between 0.529-0.627 µM C per µg XG equiv
201 L^{-1} with mean surface values being lower than at 125 m (p = 0.07, Welch's t-test) (Table 1). These values
202 are consistent with the frequently used conversion factor of 0.6 from Engel and Passow (2001). Nitrogen
203 conversion factors for CSP-N varied by a factor of ~6 between 0.003-0.018 with lower organic nitrogen
204 content found at 31ºN than at station ALOHA (p = 0.04, Welch's t-test) (Table 1.). The C:N ratio (16.4-34.3)
205 at ALOHA varied more than carbon conversion factors (0.529-0.627), e.g. by a factor of ~2 and ~1.2
206 respectively, with summertime samples from 125 m being most carbon-rich and samples from October at
207 125 m having the lowest C:N ratios (p = 0.007, Welch's t-test). All samples were carbon-rich with respect
208 to the canonical Redfield ratio, with exopolymer C:N ratios at station ALOHA being significantly higher in
209 summer than autumn at 5 m (p = 0.025, Welch's t-test) and 125 m (p = 0.007, Welch's t-test), consistent
210 with the observations of (Michaels et al., 1994). Summertime C:N ratios were significantly higher in
211 northern gyre-associated waters (31°N) than at station ALOHA, e.g. 33 – 38 vs. 26 – 34, both for 5 m (p =
212 0.0001, Welch's t-test) and at 125 m (p = 0.01, Welch's t-test).

213

214

3.2 Interannual variation in TEP, CSP, and TCHO at station ALOHA

216
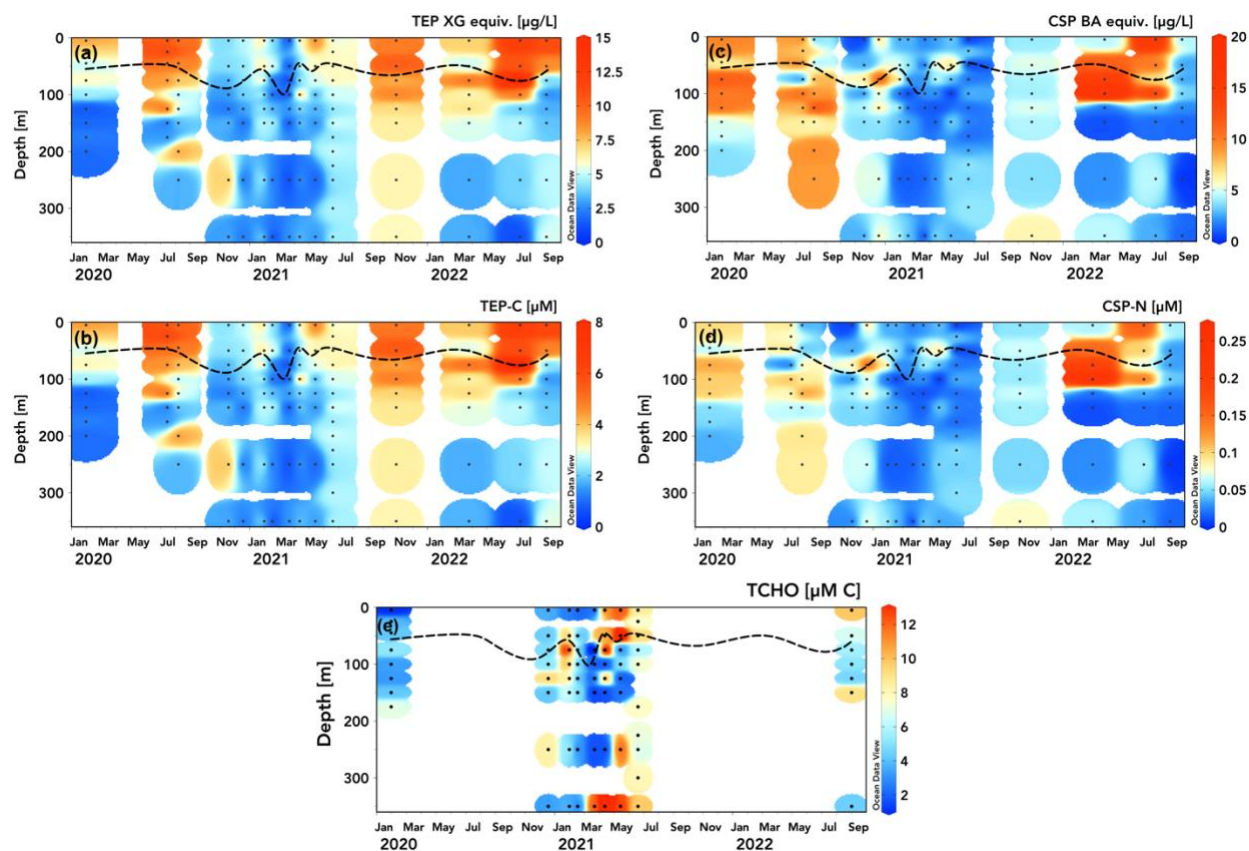
Figure 2. Station ALOHA time series (2020 – 2022) of TEP and CSP concentrations measured in xanthan gum (XG)
(a) and bovine albumin (BA) μg equivalents per litre (c) and converted to μM C (b) and μM N (d). Dissolved total
carbohydrates (TCHO) concentrations [μM C] measured on select cruises presented in (e). Dashed line shows
mixed layer depth calculated from HOT CTD data as 0.125°C decrease in temperature from the 10 m value.

At station ALOHA, TEP concentrations were highest during the summer months where values peaked
within the surface mixed layer (8 – 15 XG equiv μg L^{-1} (Fig. 2a); 4 – 8 μM C (Fig. 2b)), with decreasing TEP
concentrations below to underlying mesopelagic waters (1 – 5 XG equiv μg L^{-1} (Fig. 2a); 0.5 – 3 μM C (Fig.
2b). TEP concentrations were generally lower (2 – 7 XG equiv μg L^{-1}; 1 – 4 μM C), with less pronounced
vertical gradients during winter months, suggesting either export of accumulated TEP from surface waters
or a background of non-seasonal production or abiotic formation in deeper waters. Interannual variation
in TEP concentrations in the upper 300 m is approximately 15 – 40% (coefficient of variation), with May –
July 2021 having lower concentrations than similar periods in 2020 and 2022. March 2021 exhibited the
lowest upper 100 m concentrations (coinciding with deepening of the surface mixed layer to 110 m after
a series of storms and heavy rainfall).

The CSP distribution at station ALOHA exhibited a less observable seasonal pattern and less distinct
vertical gradients as compared to TEP (Figure 2c, 2d). Elevated CSP concentrations appear to be
distributed differently than TEP with high concentrations (6 – 18 BA equiv μg L^{-1} (Fig. 2c); 0.1 – 0.2 μM N
(Fig. 2d)) found below the surface mixed layer (50 – 100 m) and around the top of the subsurface
chlorophyll max (100-125 m), consistent with the general distributions measured by Cisternas-Novoa et
al. (2015) for the Sargasso Sea. CSP in 2021 was 2 – 8 BA equiv μg L^{-1}; 0.01 – 0.07 μM N throughout the

237 upper 300 m, similar to subsurface chlorophyll max and mesopelagic (>125 m) CSP concentrations in 2020
238 and 2022, lacking an upper ocean seasonal peak (Fig. 2c, 2d). As with TEP, CSP concentrations were
239 observed to be greater in March 2022 than post-storms in March 2021.

240 Total carbohydrate (TCHO) samples were taken on fewer HOT cruises than TEP and CSP samples during
241 2020-2022 due to logistical constraints. Total dissolved carbohydrates serve as a precursor substrate for
242 the abiotic assembly of exopolymer particles in situ (Verdugo et al., 2004). TCHO concentrations varied
243 between ~2 – 12 µM C across depths and season (Fig. 2e). There is a marked difference in the distribution
244 of TCHO concentrations between winter samples in 2020 and 2021 where surface concentrations were
245 low (2 – 6 µM) and data from spring 2021, where concentrations are consistently high at 350 m and in the
246 upper 50 m from April through June (> 10 µM). Compared to DOC measurements taken at station ALOHA,
247 this spring maximum at 350 m seems erroneous, but falls within the intra-annual variability of DOC at 350
248 m at ALOHA (± 6 µM C) and monthly variation in particulate export (Karl et al., 2021). It may be possible
249 that some hydrolysable particulate polysaccharides are drawn through combusted GF/F filters (Nagata et
250 al., 2021). Another potential explanation is the degradation and/or solubilization of exopolymers below
251 the subsurface chlorophyll max where polysaccharide-specific enzyme activity is elevated (Reintjes et al.,
252 2020).

253

254 3.3 Climatologies of TEP-C and CSP-N with Particulate Carbon and Nitrogen

255
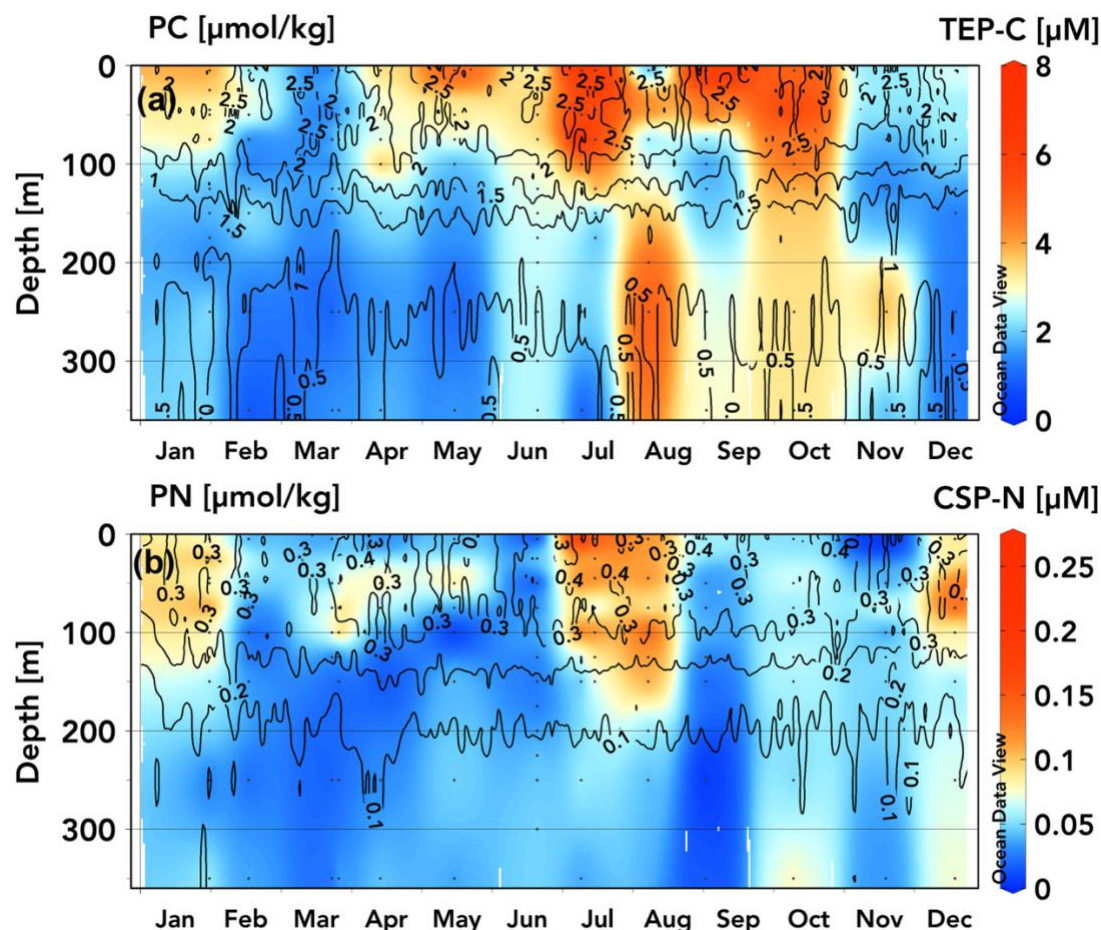
Figure 3. TEP-C (a) and CSP-N (b) (µM) concentration climatologies for 2020-2022 data measured at station ALOHA overlayed with contours from climatologies of particulate carbon (a) and particulate nitrogen (b) (µmol/kg) from the Hawaiian Ocean Time-series dataset (1989-2020 data).

Previous analyses of the climatology of upper ocean positive preNO$_3^-$ and subsurface negative preNO$_3^-$ anomaly generation at station ALOHA have revealed repeatable seasonal ingrowths of the respective anomalies during the months of April through November (Letscher and Villareal, 2018). These seasonal ingrowths are a common feature of these anomaly generation patterns across the northern hemisphere subtropics observed in the BGC-Argo float record (Smyth and Letscher, 2023). To explore exopolymer accumulation and vertical export as an explanation for these seasonal preNO$_3^-$ anomaly generation patterns, we converted the 2020-2022 TEP and CSP data to a monthly averaged climatology for station ALOHA (Figure 3), with the caveat that some months were only sampled once over the observational period. TEP exhibits a seasonal pattern with elevated concentrations found in the upper 100 m beginning in April/May (3 – 4 µM) increasing to an annual maximum in late June through early October (5 – 8 µM), followed by a decrease towards an annual minimum in February/March (1 – 2 µM) (Fig. 3a). TEP concentrations below 100 m are ~1 – 2 µM from December through June, increasing to 2 – 4 µM from June through November, concurrent with the seasonal maxima in upper 100 m TEP. We speculate that these moderate concentrations of TEP below 100 m present during summer/autumn may be due to slowly sinking aggregates as TEP accumulates in the upper 100 m through spring-summer and form aggregates before sinking, consistent with the contemporaneous peak in particulate export rates of ~30-55 mg C m^{-2} d^{-1} at station ALOHA (Emerson et al., 1997; Karl et al., 2012; Böttjer et al., 2017; Karl et al., 2021). The CSP climatology suggests two seasonal concentration maxima in the upper 100 – 130 m occurring in July/August and in December/January (0.07 – 0.13 µM) (Fig. 3b). CSP concentrations in other months and below these depths are <0.06 µM.

3.4 Patterns of TEP and CSP with respect to particulate C and N at station ALOHA
Comparing TEP and CSP concentrations to climatologies of particulate carbon (PC) and nitrogen (PN) respectively at station ALOHA (1989-2020; isolines in Fig. 3a, 3b) it is apparent that measured TEP concentrations reflect variation in euphotic PC more closely than CSP does PN, particularly for samples taken May-October. Elevated CSP-N concentrations during summer months (0.12-0.24 µM N) correspond with PN maxima, but during winter and spring, CSP-N comprises a smaller proportion of PN.

While CSP-N concentrations are lower in magnitude to PN concentrations, TEP-C is frequently observed to exceed background PC concentrations at station ALOHA, which may be an artifact of filtrations for PC and PN analysis losing exopolymers during GF/F filtration or excess dye binding to particles when using the colorimetric method of measuring TEP and CSP (Passow, 2002b; Bar-Zeev et al., 2011; Annane et al., 2015; Ortega-Retuerta et al., 2019; Nagata et al., 2021). The difference in nominal pore size between GF/F filters used to sample PC (0.7 µm) and the 0.4 µm pore-size polycarbonate filters used for TEP may also lead to sampling errors when comparing TEP-C and PC/POC, as most of these particles are small (<3 µm diameter) particularly in the upper 200 m, with particles tending larger as they age or sink and aggregate through the mesopelagic (Engel et al., 2020). It is therefore likely that TEP-C to PC ratios vary with depth and are more accurate for samples containing larger particles. Strands of microgels and larger particles may be easily pulled through GF/F filters under vacuum pressure and may be disaggregated when sampled in standard sediment catching methodology due to turbulence, break up at saline density layer, solubilization or rapid remineralization or preferential consumption by motile organisms (Smith et al., 1992; Buesseler et al., 2007; Fawcett et al., 2018). In addition to the variable size spectrum of TEP particles,

299   the electrochemistry that allows the aggregation of polymers into micro and macroscopic gels (principally
300   divalent cations Ca^{2+} and Mg^{2+}) may be affected during filtration, and to a different degree with various
301   polycarbonate and GF/F filters (Chin et al., 1998; Meers et al., 2006). If this is the case, then gels >0.4 µm
302   that would otherwise be retained may be broken apart into constituent polymers or smaller nanogels that
303   can pass through the filter. This would lead to TEP being quantified in the DOM fraction and lead to an
304   overestimate of dissolved to particulate fractions of organic matter.

305

306
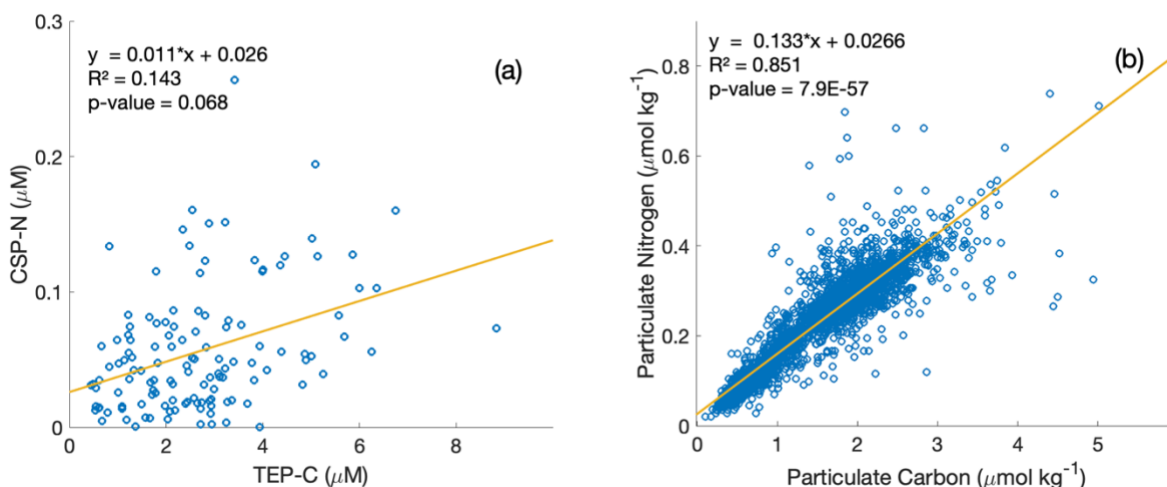
307
308   Figure 4. Property-property plots of measured CSP-N and TEP-C concentrations [µM] within the upper 350 m at
309   station ALOHA from this study (a) and particulate nitrogen to particulate carbon [µmol kg^-1] from the HOT dataset
310   (1989-2020 data) (b), including model II linear regression lines and correlation statistics.

311   We further explore the relationships between the exopolymer particle fraction, PC, and PN, and their
312   respective stoichiometries with property-property plots (Fig. 4). PN and PC concentrations are well
313   correlated (R^2 = 0.851, Model II regression) at station ALOHA (Fig. 4b) and the mean C:N ratio computed
314   from the inverse of the slope (7.55) is slightly higher than the canonical Redfield ratio (6.63). In contrast,
315   TEP-C and CSP-N concentrations show a weaker correlation (R^2 = 0.143, Model II regression), with an
316   empirical estimate of the exopolymer particle C:N stoichiometry of 90.9 or 37.3 when the regression slope
317   is forced through zero, the latter similar to the C:N stoichiometry determined directly on collected
318   exopolymers (Table 1). The weaker correlation of TEP-C with CSP-N concentrations, due to the larger
319   variability of the data, suggests different formation, consumption, and/or export dynamics for each group
320   of exopolymers, consistent with the observations of Cisternas-Novoa et al. (2015) and Zamanillo et al.
321   (2021).

322

323   3.5 TEP and rates of primary production
324
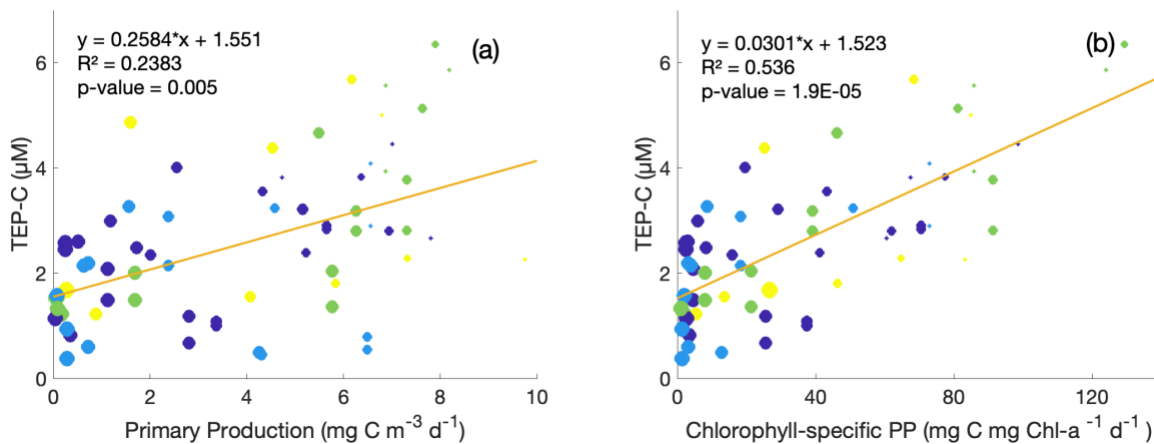
325
326 Figure 5. Property-property plots of measured TEP-C concentrations [µM C] within the upper 350 m from this study
327 against same-depth daily primary production (a) and chlorophyll-specific primary production (b) measured at
328 station ALOHA. Circle size indicates depth: larger circles are deeper samples. Colour denotes season: Purple =
329 winter, Blue = Spring, Green = Summer, Yellow = Autumn. Model II linear regression lines and correlation statistics
330 are provided.

331 As TEP production, abiotic formation, and consumption / degradation dynamics are often attributed to
332 phytoplankton community structure and downwelling irradiance intensity (Zamanillo et al., 2019; Bar-
333 Zeev et al., 2011; Ortega-Retuerta et al., 2009a; Berman-Frank et al., 2007; Passow, 2002a), daily primary
334 production (PP) measurements taken during HOT cruises were compared with TEP concentrations,
335 indicating a weak positive correlation for overall PP (R^2 = 0.24, Fig. 5a) and a stronger correlation for
336 chlorophyll-normalized PP (R^2 = 0.54, Fig. 5b). The co-occurrence of higher TEP-C concentrations and high
337 chlorophyll-specific primary production values in surface waters despite nutrient limitation may be
338 indicative of enhanced release of TEP carbohydrate precursors in addition to downregulation of
339 photosynthetic pigment synthesis in light-saturated surface waters (Rabouille et al., 2017; Thompson et
340 al., 2018). The highest values of primary productivity and TEP concentration (>4 µM) were observed in
341 Summer and Fall samples. There are too few data to determine whether TEP-C to PP ratios vary with
342 season (coloured circles, Fig. 5). CSP-N showed no such correlations with primary production within this
343 dataset. Although these results may be expected simply from the vertical gradients observed in TEP at
344 station ALOHA, chlorophyll-normalized PP gives some information on whether TEP concentrations are
345 only associated with surface accumulation or around the peak in chlorophyll at the subsurface chlorophyll
346 max. While this small dataset of TEP and PP matchups may indicate TEP production is occurring around
347 the subsurface chlorophyll max owing to moderate chlorophyll-normalized PP and TEP concentrations at
348 these depths, there are too few data at present to draw firm conclusions, particularly for near-surface
349 water. Wurl et al. (2011) found a similar disconnect between microbial activity and exopolymer
350 distributions: variations in measured TEP production rates across different Pacific waters (including late-
351 summer samples from station ALOHA) were not associated with phytoplankton blooms, changes in
352 chlorophyll concentrations or fluorescence, with abiotic formation of TEP easily maintaining observed
353 concentrations in the surface mixed layer (8-12 µM C $L^{-1} d^{-1}$).

354

355

 3.6 TEP, CSP, and TCHO concentrations on June transect 22.75°N to 31°N

357
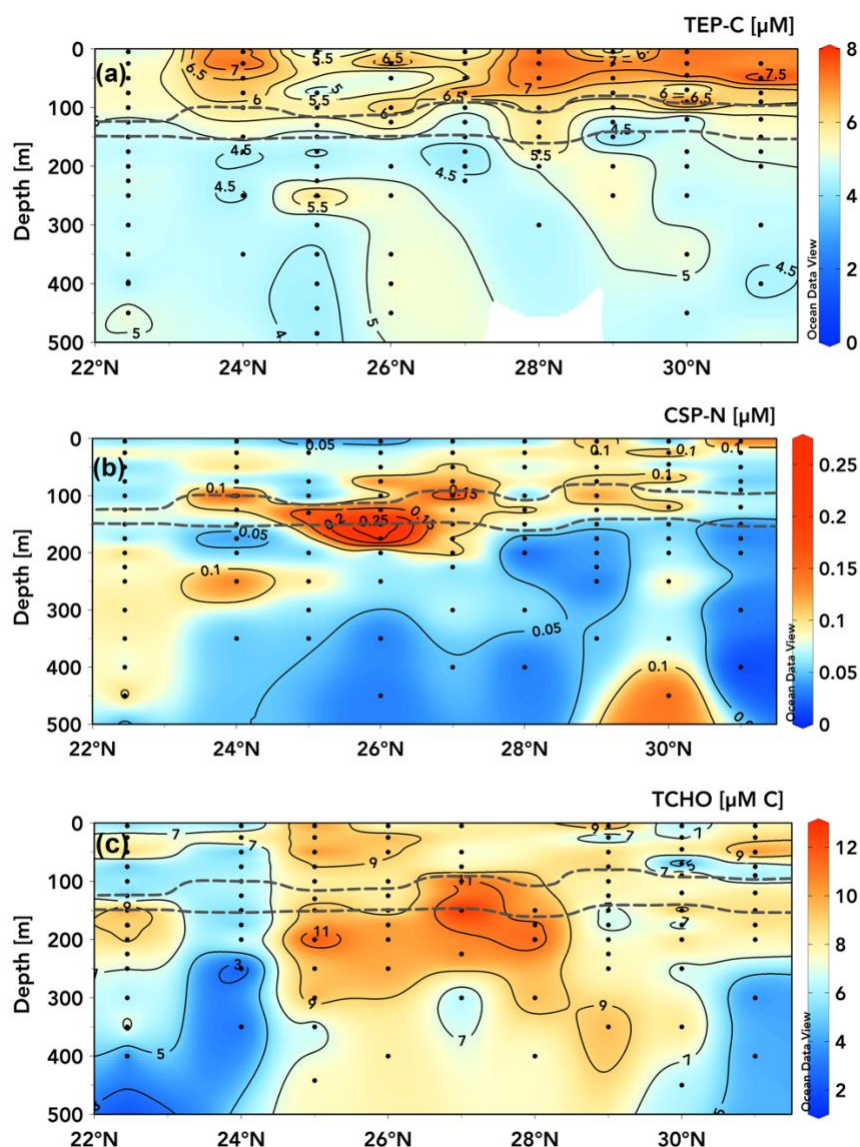
Figure 6. TEP-C [µM C] (a), CSP-N [µM N] (b), and TCHO [µM C] concentrations (with contour lines shown) within the upper 500 m measured during the June 2021 transect from 22.75°N to 31°N along ~158ºW. Dashed gray lines bound elevated CTD-mounted fluorescence, indicating the deep chlorophyll maximum.

The meridional transects of TEP-C and CSP-N concentrations in the upper 500 m taken between 22.75°N and 31°N along ~158ºW (Fig. 6) during June 2021 show an increase in upper ocean (above the subsurface chlorophyll max (gray lines, Fig. 6) TEP concentrations towards the gyre centre (Fig. 6a), with two occupations of station ALOHA at the beginning and end of the transect, separated by ten days having the lowest integrated TEP concentrations and degree of vertical gradient. From 24-31°N all stations exhibited pronounced vertical gradients in TEP concentrations between the surface and below the subsurface chlorophyll max on the order of ~2-3 µM TEP-C. At stations 24ºN and 28°N, moderate TEP-C concentrations (5.5 – 7 µM) extended into the subsurface chlorophyll max whereas high concentrations (6 – 8 µM) were restricted to the upper 75 m at 29°N and 31°N. It is unclear whether these patterns are

370   attributable to variable TEP production and consumption rates across depths, the production of buoyant
371   TEP that is retained in the surface ocean, surface turbulence and wind forcing either converging TEP to
372   certain latitudes or variably acting to break apart TEP particles, or gradients in phytoplankton nutrient or
373   oxidative stress, or photoacclimation responses affecting exudate production between sites (Sun et al.,
374   2018; Prairie et al., 2019). It is also of note that most stations exhibited a local increase in TEP-C at ~10-20
375   m immediately above the top of the subsurface chlorophyll max. The surface maxima in TEP-C present at
376   28-31ºN was ~8 µM (Fig. 6a), similar in magnitude to the surface maxima accumulating seasonally in the
377   station ALOHA time-series (Fig. 2a, 2b; 3a). However, the vertical TEP-C gradients encountered from 24-
378   31ºN in June 2021 were ~2-3 µM, approximately half that observed seasonally at station ALOHA (Fig. 2b).
379   The observed ~2 µM latitudinal gradient in 0-100 m TEP-C concentrations (e.g. ~5 µM to ~7 µM at 22.75º
380   to 24ºN and similarly at 25º to 28 – 31ºN; Fig. 6a) may also be attributed to the build-up of less labile or
381   less export-prone (or coagulation efficient) TEP as waters move towards the gyre interior (Mari et al.,
382   2007; Rochelle-Newall et al., 2010; Mari et al., 2017), a feature that is also observed for the marine DOC
383   pool (Hansell et al., 2009).

384   The meridional and vertical gradients in CSP-N concentrations (Fig. 6b) throughout the transect did not
385   correspond to those of TEP-C (Fig. 6a). CSP-N concentrations were highest (0.15-0.26 µM) between 75-
386   200 m for stations 24-29°N. Profiles at 22.75°N, 30ºN and 31ºN were more uniform with moderate CSP-N
387   concentrations (0.05 – 0.12 µM) observed below 250 m. Elevated CSP concentrations appear to be more
388   closely associated with peak fluorescence signals within the subsurface chlorophyll max (gray lines) while
389   TEP is most abundant in the surface waters above. This disconnect between TEP and CSP distributions
390   suggests different dynamics in formation, residence time and decomposition and export process between
391   the two classes of exopolymers (Grossart et al., 2006; Engel et al., 2015; Thornton, 2018).

392   Measured concentrations of total dissolved carbohydrates (TCHO) varied between ~2.5-13 µM C across
393   the June 2021 transect (Fig. 6c). Elevated TCHO concentrations did show some overlap with elevated
394   surface TEP concentrations but were not consistent with TEP concentrations below the subsurface
395   chlorophyll max (Fig. 6c). At many stations, e.g. 25º – 28ºN, TCHO concentrations were elevated (9-12.5
396   µM) around and below the subsurface chlorophyll max, where TEP-C concentrations were low (4.5-5.5
397   µM C) but CSP-N concentrations were elevated (>0.015 µM N). Most stations exhibited vertical gradients
398   between surface or subsurface chlorophyll max maxima (≥10 µM) and reduced TCHO concentrations (2
399   – 8 µM) below 250 m, but some stations were more consistent with depth (24°N, 29°N) with peak values
400   near the surface. These patterns are generally dissimilar to TEP distributions that are elevated in surface
401   waters. Measurements from this study were on the lower end of marine dissolved carbohydrate
402   measurements, but consistent with previous measurements taken within the subtropical North Pacific
403   (Pakulski and Benner, 1994), 30-60% lower than observed across the subtropical Atlantic (Burney et al.,
404   1979; Goldberg et al., 2010) and 40-100% higher than in the Bay of Bengal and Arabian Sea (Bhosle et al.,
405   1998).

406

4 Discussion

4.1 TEP, CSP, TCHO, and exopolymer C:N stoichiometry patterns at station ALOHA

A major motivation for this study of exopolymer particle dynamics at station ALOHA was to assess the potential for this organic matter pool to help explain the shallow subsurface negative, and euphotic zone positive, preNO$_3^-$ anomalies and DIC drawdown at this site, which have thus far evaded complete accounting in the relevant tracer budgets of carbon, oxygen, and nutrients (Johnson et al., 2010; Letscher and Villareal, 2018). DIC drawdown from the surface mixed layer at station ALOHA occurs from ~April through October (Keeling et al., 2004), a period of the seasonal cycle that coincides with positive preNO$_3^-$ anomaly generation in the lower euphotic zone (~40-100 m) and negative preNO$_3^-$ anomaly generation below (~100-180 m) that are in approximate stoichiometric balance (Letscher and Villareal, 2018). These preNO$_3^-$ anomalies suggest biogeochemical processes acting on the oxygen and nitrate pools that produce O$_2$ with little nitrate drawdown in the lower euphotic zone and oxygen consumption with little accumulation of nitrate below in the shallow mesopelagic. Surface ocean production/accumulation of exopolymer particles and their export and subsequent remineralization below the shallow mesopelagic is one candidate biogeochemical process that could help explain the preNO$_3^-$ anomaly generation as well as surface mixed layer DIC drawdown in the absence of nutrient injection. This would be supported if seasonal patterns of these exopolymer dynamics match the April through October timing of peak DIC and preNO$_3^-$ changes and if the exopolymer particle pool exhibits elevated C:N stoichiometry which drive comparatively larger changes in the DIC and O$_2$ pools than nitrate.

We observe a seasonal pattern for TEP concentrations at station ALOHA that includes elevated concentrations (~4-8 µM C) above ~100 m in the late spring through early fall months, with lower concentrations (~1-3 µM C) at these depths in November through March, especially in 2020-2021 (Fig. 2a, 2b), which are similar to TEP concentrations at ~100-350 m throughout the year. CSP concentrations are generally similar in pattern, however there are notable differences such as slightly deeper upper ocean maxima (e.g. from the surface down to ~120 m) and earlier seasonal peaks in the late winter early spring and seasonal lows (ending by Sep) in the upper 100 m (Fig. 2c, 2d). The limited data on the exopolymer precursor pool of dissolved TCHO precludes a complete description of the seasonal cycle, however the most elevated concentrations (~8-12 µM C) in the upper ~100 m found in early 2021 immediately precede the growth of the seasonal peak in TEP that year beginning in May (Fig. 2e, 2b). Viewed as a monthly climatology (Fig. 3a), TEP concentrations in the upper 100 m are at the annual minimum in November through March (< 3 µM C), begin to increase in concentration from April to July, and are maintained at elevated concentrations of ~4-8 µM C through October. TEP concentrations below 100 m are low (<3 µM C) year-round with the exception of some intermediate concentrations (~3-5 µM C) in the ~100-350 m depth range in July through October (Fig. 3a), more present in 2020 and 2021 than in 2022 (Fig. 2b). The seasonal upper 100 m peak in CSP is restricted to July and August in the monthly climatology (Fig. 3b) with a wintertime peak also observed (Dec – Jan), more present in 2020 than 2021 or 2022 (Fig. 2d). The empirically estimated C:N stoichiometry of the exopolymer pool in the upper 125 m is ~1.4-2.1 times more C-rich/N-poor in June 2021 than October 2021 (Table 1), suggesting that the seasonal cycles of TEP and CSP may drive a seasonal cycle in exopolymer particle stoichiometry with the most N-poor material found during summer months. All of the above seasonal patterns in euphotic zone and upper mesopelagic TEP, CSP, and exopolymer particle stoichiometry are consistent with these pools potentially helping explain the April through October patterns of surface mixed layer

450 DIC drawdown, euphotic zone positive preNO$_3^-$, and subsurface negative preNO$_3^-$ anomalies at station
451 ALOHA.

4.2 Contribution of TEP production to net community production and PreNO$_3^-$ anomalies

453 Here we use the seasonal study of TEP distributions from the upper 350 m at station ALOHA to quantify
454 its potential contribution to help explain the dual enigmas of significant net community production (DIC
455 drawdown) from the surface mixed layer in the absence of large vertical nutrient inputs and the
456 generation of preNO$_3^-$ anomalies within and immediately below the euphotic zone of the subtropical
457 North Pacific. The potential contribution of TEP to surface excess DIC drawdown and subsurface negative
458 preNO$_3^-$ anomalies under nutrient limitation has been previously identified through field and lab
459 observations (Mari et al., 2017; Fawcett et al., 2018; Letscher and Villareal, 2018; Nagata et al., 2021). The
460 seasonal ~4-6 µM TEP-C concentration gradient observed between Apr-Oct in the upper 100 m and the
461 waters below in this study at station ALOHA, may account for a significant contribution of TEP/exopolymer
462 particles to both the seasonal mixed layer net community production and upper ocean preNO$_3^-$ anomalies
463 through the processes of TEP production, sinking or matter exported during winter mixing, and
464 subsequent remineralization at depth. TEP may have a significant role in exporting low-N organic matter
465 to underlying waters, particularly during the summer to early autumn months (Fig. 3) when the seasonal
466 maximum in upper 100 m TEP concentrations extends vertically into the 100 – 300 m layer, suggestive of
467 vertical sinking.

468 The 4-6 µM vertical TEP gradient that arises seasonally at station ALOHA , e.g. 5-8 µM in the upper 100 m
469 Apr-Oct decreasing to 1-2 µM below, is higher than that observed by Cisternas-Novoa et al (2015)
470 (~10 µg XG equiv µg L^{-1} / ~0.5 µM TEP-C) in the Sargasso Sea and Wurl et al. (2011) (1.4-3.2 µM TEP-C
471 with one high-TEP station with a gradient of 27 µM TEP-C) in the subtropical North Pacific when applying
472 the carbon-converted units measured in this study. The wintertime erasure in vertical TEP gradients
473 between the surface and 200 m is observed in Feb-Mar and Nov-Dec samples from station ALOHA in this
474 study (Fig. 3a), supporting the hypothesis of TEP-C export to depth of ~100 m at ALOHA and possibly
475 deeper at latitudes further north in the subtropical North Pacific, via the seasonal mixed layer pump which
476 can deliver suspended particulate organic carbon (Dall'Olmo et al., 2016) and DOC (Hansell and Carlson,
477 2001) to sub-euphotic depths. This may operate in conjunction with the formation of sinking TEP
478 aggregates which may occur year-round (Mari et al., 2017). As its C:N stoichiometry at station ALOHA was
479 40-110% greater for summer than autumn, it seems that exported exopolymer particles from the surface
480 mixed layer to depths below may contribute disproportionally to positive and negative preNO$_3^-$ anomaly
481 generation during the summer months at elevated C:N stoichiometry, meaning respiration associated
482 with sinking exopolymers may have variable O$_2$ drawdown to nitrate release throughout the year.

483 The background particulate carbon flux at 150 m measured at station ALOHA of 27.8 ± 9.7 mg C m^2 d^{-1}
484 (845 ± 295 mmol C m^{-2} yr^{-1}; Karl et al. 2021) would seem to indicate that the export of even a portion of
485 the 0-150 m integrated 750 ± 150 mmol C m^{-2} summer/fall TEP stock by either TEP sinking or vertical
486 export following winter mixing would be a significant flux of carbon on an annual scale. Furthermore,
487 sediment trap data indicate that particulate matter exported at station ALOHA is typically slightly above
488 Redfieldian C:N proportions, e.g. ~8.0 (Hannides et al., 2009), while TEP measured in this study varied
489 between 16.4 in October to 34.3 in June (Table 1). The annual net community production rate estimated
490 from the seasonal DIC cycle within the surface mixed layer (~50 m) at Station ALOHA is 2.3 ± 0.8 mol m^{-2}
491 y^{-1} (Keeling et al., 2004), thus the annual production of a surface accumulated TEP-C stock of 0.2-0.3 mol

492 m^{-2} in the upper 50 m (e.g., ΔTEP = 4 – 6 mmol C m^{-3} multiplied by 50 m) may contribute 6.5-20% of the
493 overall net community production estimated from DIC drawdown (e.g., 0.2-0.3 divided by 2.3 ± 0.8 mol C
494 m^{-2} y^{-1}), if this material is exported below. The minimum contribution of TEP to mixed layer net community
495 production is slightly lower, ~3.5% if the seasonal ΔTEP value of ~2 mmol C m^{-3} from 2020 is used.

496 From the calculation above, TEP production within and subsequent export below the surface mixed layer
497 may explain up to 20% of the total net community production, but how does this estimate compare to
498 the estimates of 'excess' DIC drawdown, that is DIC drawdown in excess of known N inputs (Johnson et
499 al., 2010), at this site? For this calculation, it is helpful to compute the N demand required to produce the
500 observed net community production rate, partitioned amongst the relative proportions explained by the
501 production of POM and DOM. Johnson et al. (2010) computed a total N demand of 287 mmol N m^{-2} y^{-1} at
502 station ALOHA assuming total organic matter production followed a C:N stoichiometry of 8.0, matching
503 the sinking POM stoichiometry (Hannides et al., 2009). Letscher & Villareal (2018) empirically determined
504 the fraction of net community production partitioned to DOM at station ALOHA from tracer budgets in
505 upper mesopelagic isopycnal layers from the station ALOHA climatology, finding that ~50% of net
506 community production is exported as DOM. We have computed the mean DOM C:N stoichiometry in the
507 upper 200 m at 15.5 ± 1.3 from the same climatology. Assuming net community production is partitioned
508 50/50% between POM and DOM with C:N stoichiometries of 8.0 and 15.5 respectively, we compute a
509 revised N demand of 218 mmol N m^{-2} y^{-1} to satisfy the observed 2.3 mol C m^{-2} y^{-1} net community
510 production within the mixed layer (Keeling et al., 2004) for the scenario whereby only POM and DOM
511 contribute to export production. Johnson et al. (2010) summarized total N supply to the mixed layer at
512 station ALOHA finding a magnitude of 144 – 201 mmol N m^{-2} y^{-1}. Thus approximately 8 – 34% (mean =
513 21%) of the observed net community production N requirement is not accounted for by the known N
514 supply (i.e. 'unexplained') for the scenario whereby only POM and DOM export contribute to net
515 community production. Our study suggests that exopolymer particles may contribute as a third organic
516 matter pool that can be exported to balance net community production. Our estimate of TEP production
517 and its contribution to net community production at this site is 6.5 – 20%, with an observationally
518 determined C:N stoichiometry of 16.4 – 34.3 (Table 1). Addition of TEP into the surface mixed layer net
519 community production budget yields an N demand to explain TEP production of 4 – 28 mmol N m^{-2} y^{-1},
520 which reduces the revised total N demand of 218 mmol N m^{-2} y^{-1} (after accounting for elevated C:N DOM)
521 even further downwards to 174 – 208 mmol N m^{-2} y^{-1}. Comparing this N demand to the prior calculated N
522 demand that included POM and DOM but ignored TEP, TEP contributions to the upper ocean net
523 community production budget help explain ~57% of the 'unexplained' excess DIC drawdown from the
524 surface mixed layer, i.e. by reducing the overall unexplained drawdown from a mean of ~21% to ~9%,
525 estimated from comparing the revised N demand for an upper ocean ecosystem including TEP production
526 of 174-208 mmol N m^{-2} y^{-1} to the estimated N supply of 144-201 mmol N m^{-2} y^{-1} at station ALOHA (Johnson
527 et al., 2010).

528 Table 2. Estimates of the nitrogen demand partitioned amongst POM, DOM, and TEP required to satisfy each
529 fractional contribution (fNCP) of the mixed layer 2.3 mol m^{-2} y^{-1} net community production at station ALOHA using
530 their respective C:N stoichiometries. Total N supply is taken from Johnson et al. (2010) and includes vertical NO$_3$
531 fluxes plus N$_2$ fixation. fNCP$_{POM}$ varies as the particulate fraction not attributable to TEP or DOM (fNCP$_{POM}$ = 1-(fNCP$_{TEP}$
532 + fNCP$_{DOM}$)), POM C:N from Hannides et al. (2009), fNCP$_{DOM}$ from Letscher and Villareal (2018), DOM C:N from the
533 upper 200 m average of the station ALOHA climatology, fNCP$_{TEP}$ and TEP C:N (Table 1) from this study. N demand
534 computed from 2.3 mol C m^{-2} yr^{-1} divided by C:N multiplied by fNCP.

Depth integration		^{f}NCP	C:N	N demand (mmol N m^{-2} yr^{-1})	% of N demand
50m	POM	0.30-0.435	8	86-125	36-52
	DOM	0.5	15.5	74	31
	TEP	0.065-0.20	16.4-34.3	4-28	2-12
	Total demand			**174-208**	
	Total supply			**144-201**	

535

536 Lastly, we compare the seasonal TEP cycle observed at station ALOHA from 2020-2022 to previous
537 estimates of the formation rates of residual preNO$_3^-$ anomalies within and immediately below the
538 euphotic zone. Letscher and Villareal (2018) estimated the seasonal (~Apr-Oct) development of a residual
539 positive preNO$_3^-$ anomaly (i.e. the residual anomaly after accounting for non-Redfield POM and DOM
540 stoichiometry) within the upper 100 m with a climatological magnitude of 0.53 ± 0.27 µM N. A similar
541 seasonal negative preNO$_3^-$ anomaly develops between ~100-180 m with a climatological magnitude of -
542 0.54 ± 0.25 µM N over a ~180-day period from Apr-Oct, consistent with surface TEP accumulation before
543 winter mixing (Fig. 2). With an assumed 1:1 C:O$_2$ stoichiometry of TEP formation and remineralization (as
544 for nearly pure carbohydrate material), the consumption of 4-6 µM seasonally exported TEP C (at a C:N
545 ratio of 25 ± 8) should release the equivalent of 0.12-0.35 µM nitrate which is 23-67% of the 0.53 µM
546 mean residual negative preNO$_3^-$ anomaly and 22-64% of the 0.54 µM mean residual positive preNO$_3^-$
547 anomaly. These values for TEP's potential contribution to preNO$_3^-$ anomalies assume the export of surface
548 TEP to underlying waters 100-200 m where they are subsequently remineralized. If a large proportion of
549 seasonal TEP production is quickly exported to the deeper mesopelagic through aggregation and
550 gravitational settling or winter mixing, then these values will likely be overestimates. Remaining
551 mechanisms to explain the remainder of preNO$_3^-$ anomaly formation include mining of sub-euphotic zone
552 nitrate by vertically migrating phytoplankton (Pilskaln et al., 2005; Villareal et al., 2014) and heterotrophic
553 bacterial uptake of nitrate when consuming C-rich organic matter such as TEP (Fawcett et al., 2018).

554 Finally, we note that moderate concentrations of TEP at 150-350 m (3-5 µM C) are present throughout
555 the late summer to early autumn months at station ALOHA (Fig. 2b, Fig. 3a), but whether these
556 concentrations represent matter exported from the surface or subsurface chlorophyll max below the
557 depth of the negative preNO$_3^-$ anomaly (~100 – 180 m; Letscher & Villareal, 2018), or separate activity in
558 the upper mesopelagic is unclear. Compositional analysis of TEP molecules and polysaccharide-associated
559 enzymes throughout the water column and over an annual cycle may elucidate sources and sinks of TEP
560 beyond physical sinking and mixing processes.

561 ## 4.3 TEP, CSP, and TCHO meridional patterns in the NPSG

562 Previous observations of TEP and CSP particle concentrations in high latitude oceans and temperate shelf
563 seas have observed that both exopolymers are coupled to chlorophyll distributions (Beauvais et al., 2003;
564 Busch et al., 2017; Nosaka et al., 2017; Anastasi, n.d.; von Jackowski et al., 2020). Other mid-latitude
565 regions such as the Sargasso Sea (Cisternas-Novoa et al., 2015) and Catalan Sea (Zamanillo et al., 2021)
566 exhibit different dynamics, where TEP is disconnected from CSP distributions as was observed in this study
567 in the subtropical North Pacific.

568 Exopolymers measured across the upper 500 m of the subtropical North Pacific in June 2021 (Fig. 6) were
569 found to have depth gradients similar to summertime conditions at station ALOHA (Fig. 2, 3), with elevated
570 concentrations in surface waters for TEP and around the subsurface chlorophyll max for CSP and lower
571 concentrations below in the shallow mesopelagic. There are also meridional gradients present (Fig. 6) with
572 increasing surface ocean TEP concentrations northwards towards 31ºN while CSP is most elevated at 24
573 – 30ºN. Without additional data on TEP/exopolymer molecular composition it is difficult to ascertain
574 whether this meridional gradient represents accumulation of more refractory TEP, or enhanced
575 production/depressed export from waters towards 31ºN. However, this TEP meridional gradient matches
576 that observed for surface ocean DOC in the region (Abell et al., 2000) which is thought to arise from the
577 convergence of a semilabile component of DOC with lifetimes of years by the Ekman circulation across
578 subtropical gyres (Hansell et al., 2009). The C:N stoichiometry of the exopolymer particle pool was also
579 found to increase from station ALOHA to 31ºN both at the surface (~26 vs. ~33) and at 125 m (~34 vs. ~38)
580 (Table 1). Dissolved TCHO were more elevated (> 7 µM C) north of 24ºN as well (Fig. 6c). The observed
581 disconnect between TEP and TCHO distributions may be attributed to both formation and degradation
582 processes: precursors being created around the subsurface chlorophyll max by phytoplankton and
583 resultant low-density TEP particles concentrating in surface waters or sinking TEP being hydrolyzed below
584 the subsurface chlorophyll max by bacteria, yielding reduced TCHO concentrations. The latter process is
585 consistent with the hypothesized remineralization of low-N organic matter requiring heterotrophic nitrate
586 uptake, generating a negative preNO$_3^-$ anomaly (Fawcett et al., 2018). Compositional analysis of TEP
587 particles, dissolved sugars, and stable isotopic measurements of the relevant nutrient and organic matter
588 N contents through the upper 400 m would help confirm. Lastly, a lack of spatiotemporal coherence in
589 the distributions of TEP and its precursor TCHO may result from differing timescales over which they are
590 biotically cycled, with the latter possibly processed 3-10 times faster than other common labile organic
591 materials like amino acids by bacteria in open ocean environments (Kaiser and Benner, 2012).

592 The meridional patterns observed in TEP, CSP, TCHO, and exopolymer particle C:N stoichiometry are all
593 suggestive that the contributions of exopolymer particle dynamics to upper ocean net community
594 production, export, and nutrient cycling diagnosed at station ALOHA (Sect 4.2) may play a larger role
595 further north towards the core of the subtropical North Pacific gyre. While the TEP concentrations
596 measured in this study were low (~2-15 XG equiv. µg/L; 1-8 µM C) compared to other regions (e.g. ~20-40
597 XG equiv. µg/L in the Sargasso Sea (Cisternas-Novoa et al., 2015); ~1-20 µM C in the tropical North Pacific
598 (Wurl et al., 2011)), their highly carbon-enriched stoichiometry (particularly in summer with C:N = 26-38)
599 means that these particles are a significant component of the upper ocean organic matter pool. The
600 seasonal and latitudinal variation we observed in carbon and nitrogen conversion factors suggest using a
601 single factor will bias many estimates of TEP-C and CSP-N from dye-binding assays. We therefore hope
602 that more effort will be made in future studies to constrain TEP and CSP elemental stoichiometry to
603 compare exopolymer concentrations from different depths, seasons and locations with greater
604 confidence.

605

5 Conclusions and Future Directions

607 The seasonal, interannual and meridional variation of TEP and CSP observed in this study reinforces the
608 building evidence that exopolymer production, accumulation and remineralization are not static
609 processes, even in oligotrophic regions (Radić et al., 2006; Cisternas-Novoa et al., 2015; Engel et al., 2015;

610   Zäncker et al., 2017). Further process experiments that incorporate TEP and CSP dynamics with respect to
611   other biological and chemical parameters are needed to understand the biogeochemistry of each
612   exopolymer type for a given location and season, aiding efforts to model both with respect to other
613   parameters through depth and time at a synoptic scale. Work that helps to validate the sources and sinks
614   of exopolymers within the water column is particularly important in quantifying how much carbon is
615   exported from or cycled within surface waters (including the surface microlayer) and where these
616   molecules are remineralized. Compositional analysis of TEP particle and dissolved carbohydrates
617   compositions and associated proteomic or transcriptomic analyses may elucidate the vertical distribution
618   of TEP production, enzymatic hydrolyzation and remineralization of the resulting labile monomeric sugars.

619   TEP concentrations measured with the Alcian blue spectrophotometric method and converted to μM C
620   with our empirically derived carbon conversion factors were found to be greater than GF/F collected
621   particulate carbon measurements from the Hawaiian Ocean Time-series. Additionally, the estimated C:N
622   stoichiometry of 16.4 – 38.1 for exopolymer particles from this study is significantly C-rich/N-poor relative
623   to the C:N of the sinking flux collected in sediment traps at station ALOHA, 8.0 (Hannides et al., 2009). This
624   supports the hypotheses that TEP and marine microgels may be 'missed' by traditional sampling
625   techniques for sinking and suspended particulate organic carbon (Quigg et al., 2021), possibly due to
626   disaggregation of the gel-particles upon encountering the GF/F filter or collection brine of sediment traps
627   as well as potential rapid microbial remineralization within trap cups (Fawcett et al., 2018 and references
628   therein). Future research is required to resolve the mechanisms leading to inefficient collection of TEP
629   within standard marine particle sampling protocols and fully integrate TEP and marine gels sampling
630   within marine carbon biogeochemistry studies. Further work is also needed to ascertain the degree to
631   which exopolymer particles are exported below the surface ocean via slow gravitational sinking and/or
632   vertical mixing within the seasonal mixed layer pump (Quigg et al., 2021; Mari et al., 2017).

633   Following the conversion of semi-quantitative measurements of exopolymers from dye-binding assays,
634   our elemental conversions to C and N units allow us to estimate the magnitude of TEP's importance to
635   surface ocean carbon dynamics on an annual cycle. We estimate that TEP accumulation within the ~50 m
636   mixed layer may constitute 6.5-20% (0.2-0.3 mol m^{-2} y^{-1}) of the net community production (2.3 ± 0.8 mol
637   m^{-2} y^{-1}) at station ALOHA. With its low N requirement, TEP reduces the overall N demand needed to explain
638   the observed net community production at this site, bringing the measured N supply and demand into
639   near balance. If TEP is sufficiently exported below the euphotic zone by a combination of sinking and/or
640   winter vertical mixing, its cycling can reduce the unexplained 'excess' DIC drawdown from the mixed layer
641   by ~57%, bringing the overall unexplained excess (or missing N supply) to ~9%.

642   Though TEP sinking rates, remineralization rates and C:O_2 respiration stoichiometry are not addressed in
643   this dataset, previous studies in analogous regions indicate that the summertime production of highly
644   non-Redfieldian exopolymers and potential winter export observed in this time series may explain a
645   significant portion of subtropical positive and negative $preNO_3^-$ anomalies (22-67%), consistent with this
646   mechanism's description and modelling by Letscher and Villareal (2018). Uncertainty in the contribution
647   of TEP/exopolymers to $preNO_3^-$ anomalies (and excess DIC drawdown) primarily results from variability in
648   the total TEP upper ocean accumulation and its C:N ratio; with some evidence for seasonal, vertical, and
649   meridional differences in these ratios evidenced in this study. The upper ocean exopolymer cycle helps to
650   close the C, N, and O_2 budgets at station ALOHA, while leaving room for significant contributions from
651   other processes such as vertically migrating phytoplankton and heterotrophic nitrate uptake to be further
652   validated. More frequent measurements of TEP concentrations and its stoichiometry from the subtropical

653 North Pacific and elsewhere would help quantify this potentially overlooked component of the ocean's
654 biological pump operating across the vast subtropical gyres. .

655

656 **Author contributions**

657 RTL and TV conceptualized this study as part of NSF grants 1923687 and 1923667 "Transparent
658 exopolymer and phytoplankton vertical migration as sources for preformed nitrate anomalies in the
659 subtropical N. Pacific Ocean". KC, RTL, and HOT technicians performed fieldwork; KC performed
660 laboratory analyses for TEP, CSP and TCHO and respective data analyses. KC, RTL, and TV contributed to
661 writing and editing. Data from the Hawaiian Ocean Time series were obtained via the Hawaii Ocean Time-
662 series HOT-DOGS application; University of Hawai'i at Mānoa. National Science Foundation Award #
663 1756517.

664 **Acknowledgements**

665 We would like to thank the crew and technicians aboard the RV Kilo Moana for their assistance in
666 collecting samples through the COVID pandemic and assisting during the June 2021 transect cruise. We
667 are grateful to Angelicque White (UH-Manoa) for her assistance and leadership in accommodating the
668 TEP, CSP, and TCHO sampling on the 2020-2022 HOT cruises and to Brandon Brenes (UH-Manoa) for much
669 of the sample collection at sea. We also wish to thank former UNH graduate students Jessica Gray and
670 Sarah Benson for their assistance with sampling during the 2021 cruise.

671

672 **Financial support**

673 This study was funded as part of NSF grant 1923687 to RTL and 1923667 to TV entitled: "Collaborative
674 research: Transparent exopolymer and phytoplankton vertical migration as sources for preformed nitrate
675 anomalies in the subtropical N. Pacific Ocean."

676

677 **Data availability**

678 The data reported in this study are available at: https://www.bco-dmo.org/project/772658.

679

680 **Competing interests**

681 We declare no competing interests in the undertaking and publication of this study.

682

References

684 Abell, J., Emerson, S., and Keil, R. G.: Using preformed nitrate to infer decadal changes in DOM
685 remineralization in the subtropical North Pacific, Glob. Biogeochem. Cycles, 19,
686 https://doi.org/10.1029/2004GB002285, 2005.

687   Aller, J. Y., Radway, J. C., Kilthau, W. P., Bothe, D. W., Wilson, T. W., Vaillancourt, R. D., Quinn, P. K.,
688   Coffman, D. J., Murray, B. J., and Knopf, D. A.: Size-resolved characterization of the polysaccharidic and
689   proteinaceous components of sea spray aerosol, Atmos. Environ., 154, 331–347,
690   https://doi.org/10.1016/j.atmosenv.2017.01.053, 2017.

691   Anastasi, G.: OBSERVATIONS AND MODELLING OF TRANSPARENT EXOPOLYMER PARTICLES (TEP) AND
692   THEIR ROLE IN CARBON CYCLING IN SHELF SEAS, 237, n.d.

693   Annane, S., St-Amand, L., Starr, M., Pelletier, E., and Ferreyra, G. A.: Contribution of transparent
694   exopolymeric particles (TEP) to estuarine particulate organic carbon pool, Mar. Ecol. Prog. Ser., 529, 17–
695   34, https://doi.org/10.3354/meps11294, 2015.

696   Arnosti, C., Wietz, M., Brinkhoff, T., Hehemann, J.-H., Probandt, D., Zeugner, L., and Amann, R.: The
697   Biogeochemistry of Marine Polysaccharides: Sources, Inventories, and Bacterial Drivers of the
698   Carbohydrate Cycle, Annu. Rev. Mar. Sci., 13, 81–108, https://doi.org/10.1146/annurev-marine-032020-
699   012810, 2021.

700   Ascani, F., Richards, K. J., Firing, E., Grant, S., Johnson, K. S., Jia, Y., Lukas, R., and Karl, D. M.: Physical and
701   biological controls of nitrate concentrations in the upper subtropical North Pacific Ocean, Deep Sea Res.
702   Part II Top. Stud. Oceanogr., 93, 119–134, https://doi.org/10.1016/j.dsr2.2013.01.034, 2013.

703   Azetsu-Scott, K. and Passow, U.: Ascending marine particles: Significance of transparent exopolymer
704   particles (TEP) in the upper ocean, Limnol. Oceanogr., 49, 741–748,
705   https://doi.org/10.4319/lo.2004.49.3.0741, 2004.

706   Bar-Zeev, E., Berman, T., Rahav, E., Dishon, G., Herut, B., Kress, N., and Berman-Frank, I.: Transparent
707   exopolymer particle (TEP) dynamics in the eastern Mediterranean Sea, Mar. Ecol. Prog. Ser., 431, 107–
708   118, https://doi.org/10.3354/meps09110, 2011.

709   Beauvais, S., Pedrotti, M. L., Villa, E., and Lemée, R.: Transparent exopolymer particle (TEP) dynamics in
710   relation to trophic and hydrological conditions in the NW Mediterranean Sea, Mar. Ecol. Prog. Ser., 262,
711   97–109, https://doi.org/10.3354/meps262097, 2003.

712   Berman-Frank, I., Rosenberg, G., Levitan, O., Haramaty, L., and Mari, X.: Coupling between autocatalytic
713   cell death and transparent exopolymeric particle production in the marine cyanobacterium
714   Trichodesmium, Environ. Microbiol., 9, 1415–1422, https://doi.org/10.1111/j.1462-2920.2007.01257.x,
715   2007.

716   Bhosle, N. B., Bhaskar, P. V., and Ramachandran, S.: Abundance of dissolved polysaccharides in the
717   oxygen minimum layer of the Northern Indian Ocean, Mar. Chem., 63, 171–182,
718   https://doi.org/10.1016/S0304-4203(98)00061-9, 1998.

719   Böttjer, D., Dore, J. E., Karl, D. M., Letelier, R. M., Mahaffey, C., Wilson, S. T., Zehr, J., and Church, M. J.:
720   Temporal variability of nitrogen fixation and particulate nitrogen export at Station ALOHA, Limnol.
721   Oceanogr., 62, 200–216, https://doi.org/10.1002/lno.10386, 2017.

722   Buesseler, K. O., Antia, A. N., Chen, M., Fowler, S. W., Gardner, W. D., Gustafsson, O., Harada, K.,
723   Michaels, A. F., Rutgers van der Loeff, M., Sarin, M., Steinberg, D. K., and Trull, T.: An assessment of the

724 use of sediment traps for estimating upper ocean particle fluxes, J. Mar. Res., 65, 345–416,
725 https://doi.org/10.1357/002224007781567621, 2007.

726 Burney, C. M., Johnson, K. M., Lavoie, D. M., and Sieburth, J. McN.: Dissolved carbohydrate and
727 microbial ATP in the North Atlantic: concentrations and interactions, Deep Sea Res. Part Oceanogr. Res.
728 Pap., 26, 1267–1290, https://doi.org/10.1016/0198-0149(79)90068-2, 1979.

729 Busch, K., Endres, S., Iversen, M. H., Michels, J., Nöthig, E.-M., and Engel, A.: Bacterial Colonization and
730 Vertical Distribution of Marine Gel Particles (TEP and CSP) in the Arctic Fram Strait, Front. Mar. Sci., 4,
731 2017.

732 Chin, W.-C., Orellana, M. V., and Verdugo, P.: Spontaneous assembly of marine dissolved organic matter
733 into polymer gels, Nature, 391, 568–572, https://doi.org/10.1038/35345, 1998.

734 Chow, C. H., Cheah, W., and Tai, J.-H.: A rare and extensive summer bloom enhanced by ocean eddies in
735 the oligotrophic western North Pacific Subtropical Gyre, Sci. Rep., 7, 6199,
736 https://doi.org/10.1038/s41598-017-06584-3, 2017.

737 Cisternas-Novoa, C., Lee, C., and Engel, A.: Transparent exopolymer particles (TEP) and Coomassie
738 stainable particles (CSP): Differences between their origin and vertical distributions in the ocean, Mar.
739 Chem., 175, 56–71, https://doi.org/10.1016/j.marchem.2015.03.009, 2015.

740 Dall'Olmo, G., Dingle, J., Polimene, L., Brewin, R. J., & Claustre, H. (2016). Substantial energy input to the
741 mesopelagic ecosystem from the seasonal mixed-layer pump. *Nature Geoscience*, *9*(11), 820-823.

742 Dave, A. C. and Lozier, M. S.: Local stratification control of marine productivity in the subtropical North
743 Pacific, J. Geophys. Res. Oceans, 115, https://doi.org/10.1029/2010JC006507, 2010.

744 Emerson, S.: Annual net community production and the biological carbon flux in the ocean, Glob.
745 Biogeochem. Cycles, 28, 14–28, https://doi.org/10.1002/2013GB004680, 2014.

746 Emerson, S. and Hayward, T.: Chemical tracers of biological processes in shallow waters of North Pacific:
747 preformed nitrate distributions., J. Mar. Res., 53, 499–513, 1995.

748 Emerson, S., Quay, P., Karl, D., Winn, C., Tupas, L., and Landry, M.: Experimental determination of the
749 organic carbon flux from open-ocean surface waters, Nature, 389, 951–954,
750 https://doi.org/10.1038/40111, 1997.

751 Engel, A. and Passow, U.: Carbon and nitrogen content of transparent exopolymer particles (TEP) in
752 relation to their Alcian Blue adsorption, Mar. Ecol. Prog. Ser., 219, 1–10,
753 https://doi.org/10.3354/meps219001, 2001.

754 Engel, A., Borchard, C., Loginova, A., Meyer, J., Hauss, H., and Kiko, R.: Effects of varied nitrate and
755 phosphate supply on polysaccharidic and proteinaceous gel particle production during tropical
756 phytoplankton bloom experiments, Biogeosciences, 12, 5647–5665, https://doi.org/10.5194/bg-12-
757 5647-2015, 2015.

758 Engel, A., Endres, S., Galgani, L., and Schartau, M.: Marvelous Marine Microgels: On the Distribution and
759 Impact of Gel-Like Particles in the Oceanic Water-Column, Front. Mar. Sci., 7,
760 https://doi.org/10.3389/fmars.2020.00405, 2020.

761 Fawcett, S. E., Johnson, K. S., Riser, S. C., Van Oostende, N., and Sigman, D. M.: Low-nutrient organic
762 matter in the Sargasso Sea thermocline: A hypothesis for its role, identity, and carbon cycle implications,
763 Mar. Chem., 207, 108–123, https://doi.org/10.1016/j.marchem.2018.10.008, 2018.

764 Goldberg, S. J., Carlson, C. A., Bock, B., Nelson, N. B., and Siegel, D. A.: Meridional variability in dissolved
765 organic matter stocks and diagenetic state within the euphotic and mesopelagic zone of the North
766 Atlantic subtropical gyre, Mar. Chem., 119, 9–21, https://doi.org/10.1016/j.marchem.2009.12.002,
767 2010.

768 Grossart, H.-P., Czub, G., and Simon, M.: Algae–bacteria interactions and their effects on aggregation
769 and organic matter flux in the sea, Environ. Microbiol., 8, 1074–1084, https://doi.org/10.1111/j.1462-
770 2920.2006.00999.x, 2006.

771 Gruber, N., Keeling, C. D., and Stocker, T. F.: Carbon-13 constraints on the seasonal inorganic carbon
772 budget at the BATS site in the northwestern Sargasso Sea, Deep Sea Res. Part Oceanogr. Res. Pap., 45,
773 673–717, https://doi.org/10.1016/S0967-0637(97)00098-8, 1998.

774 Guo, S., Wu, Y., Zhu, M., and Sun, X.: Concentrations of transparent exopolymer particles (TEPs) and
775 their role in the carbon export in the South China Sea and western tropical North Pacific, Mar. Environ.
776 Res., 179, 105699, https://doi.org/10.1016/j.marenvres.2022.105699, 2022.

777 Hannides, C. C. S., Popp, B. N., Landry, M. R., and Graham, B. S.: Quantification of zooplankton trophic
778 position in the North Pacific Subtropical Gyre using stable nitrogen isotopes, Limnol. Oceanogr., 54, 50–
779 61, https://doi.org/10.4319/lo.2009.54.1.0050, 2009.

780 Hansell, D. A., & Carlson, C. A. (2001). Biogeochemistry of total organic carbon and nitrogen in the
781 Sargasso Sea: control by convective overturn. *Deep Sea Research Part II: Topical Studies in*
782 *Oceanography*, *48*(8-9), 1649-1667.

783 Hansell, D. A., Carlson, C. A., Repeta, D. J., & Schlitzer, R. (2009). Dissolved organic matter in the ocean:
784 A controversy stimulates new insights. *Oceanography*, *22*(4), 202-211.

785 Iuculano, F., Mazuecos, I. P., Reche, I., and Agustí, S.: Prochlorococcus as a Possible Source for
786 Transparent Exopolymer Particles (TEP), Front. Microbiol., 8, 2017.

787 von Jackowski, A., Grosse, J., Nöthig, E.-M., and Engel, A.: Dynamics of organic matter and bacterial
788 activity in the Fram Strait during summer and autumn, Philos. Trans. R. Soc. Math. Phys. Eng. Sci., 378,
789 20190366, https://doi.org/10.1098/rsta.2019.0366, 2020.

790 Johnson, K. S., Riser, S. C., and Karl, D. M.: Nitrate supply from deep to near-surface waters of the North
791 Pacific subtropical gyre, Nature, 465, 1062–1065, https://doi.org/10.1038/nature09170, 2010.

792 Kaiser, K. and Benner, R.: Organic matter transformations in the upper mesopelagic zone of the North
793 Pacific: Chemical composition and linkages to microbial community structure, J. Geophys. Res. Oceans,
794 117, https://doi.org/10.1029/2011JC007141, 2012.

795 Karl, D. M., Church, M. J., Dore, J. E., Letelier, R. M., and Mahaffey, C.: Predictable and efficient carbon
796 sequestration in the North Pacific Ocean supported by symbiotic nitrogen fixation, Proc. Natl. Acad. Sci.,
797 109, 1842–1849, https://doi.org/10.1073/pnas.1120312109, 2012.

798 Karl, D. M., Letelier, R. M., Bidigare, R. R., Björkman, K. M., Church, M. J., Dore, J. E., and White, A. E.:
799 Seasonal-to-decadal scale variability in primary production and particulate matter export at Station
800 ALOHA, Prog. Oceanogr., 195, 102563, https://doi.org/10.1016/j.pocean.2021.102563, 2021.

801 Keeling, C. D., Brix, H., and Gruber, N.: Seasonal and long-term dynamics of the upper ocean carbon
802 cycle at Station ALOHA near Hawaii, Glob. Biogeochem. Cycles, 18,
803 https://doi.org/10.1029/2004GB002227, 2004.

804 Lamborg, C. H., Buesseler, K. O., Valdes, J., Bertrand, C. H., Bidigare, R., Manganini, S., Pike, S., Steinberg,
805 D., Trull, T., and Wilson, S.: The flux of bio- and lithogenic material associated with sinking particles in
806 the mesopelagic "twilight zone" of the northwest and North Central Pacific Ocean, Deep Sea Res. Part II
807 Top. Stud. Oceanogr., 55, 1540–1563, https://doi.org/10.1016/j.dsr2.2008.04.011, 2008.

808 Letelier, R. M., Björkman, K. M., Church, M. J., Hamilton, D. S., Mahowald, N. M., Scanza, R. A.,
809 Schneider, N., White, A. E., and Karl, D. M.: Climate-driven oscillation of phosphorus and iron limitation
810 in the North Pacific Subtropical Gyre, Proc. Natl. Acad. Sci., 116, 12720–12728,
811 https://doi.org/10.1073/pnas.1900789116, 2019.

812 Letscher, R. T. and Villareal, T. A.: Evaluation of the seasonal formation of subsurface negative
813 preformed nitrate anomalies in the subtropical North Pacific and North Atlantic, Biogeosciences, 15,
814 6461–6480, https://doi.org/10.5194/bg-15-6461-2018, 2018.

815 Liang, Z., Letscher, R. T., and Knapp, A. N.: Global patterns of surface ocean dissolved organic matter
816 stoichiometry, *Global Biogeochemical Cycles*, *37*(12), e2023GB007788,
817 https://doi.org/10.1029/2023GB007788, 2023.

818 Ling, S. C. and Alldredge, A. L.: Does the marine copepod Calanus pacificus consume transparent
819 exopolymer particles (TEP)?, J. Plankton Res., 25, 507–515, https://doi.org/10.1093/plankt/25.5.507,
820 2003.

821 Long, J., Fassbender, A., and Estapa, M.: Depth-Resolved Net Primary Production in the Northeast Pacific
822 Ocean: A Comparison of Satellite and Profiling Float Estimates in the Context of Two Marine Heatwaves,
823 Geophys. Res. Lett., 48, https://doi.org/10.1029/2021GL093462, 2021.

824 Longhurst, A., Sathyendranath, S., Platt, T., and Caverhill, C.: An estimate of global primary production in
825 the ocean from satellite radiometer data, J. Plankton Res., 17, 1245–1271,
826 https://doi.org/10.1093/plankt/17.6.1245, 1995.

827 Mari, X., Beauvais, S., Lemée, R., and Pedrotti, M. L.: Non-Redfield C:N ratio of transparent exopolymeric
828 particles in the northwestern Mediterranean Sea, Limnol. Oceanogr., 46, 1831–1836,
829 https://doi.org/10.4319/lo.2001.46.7.1831, 2001.

830 Mari, X., Rochelle-Newall, E., Torréton, J.-P., Pringault, O., Jouon, A., and Migon, C.: Water residence
831 time: A regulatory factor of the DOM to POM transfer efficiency, Limnol. Oceanogr., 52, 808–819,
832 https://doi.org/10.4319/lo.2007.52.2.0808, 2007.

Mari, X., Passow, U., Migon, C., Burd, A. B., and Legendre, L.: Transparent exopolymer particles: Effects on carbon cycling in the ocean, Prog. Oceanogr., 151, 13–37, https://doi.org/10.1016/j.pocean.2016.11.002, 2017.

McCarthy, M., Hedges, J., and Benner, R.: Major biochemical composition of dissolved high molecular weight organic matter in seawater, Mar. Chem., 55, 281–297, https://doi.org/10.1016/S0304-4203(96)00041-2, 1996.

Meers, E., Laing, G. D., Unamuno, V. G., Lesage, E., Tack, F. M. G., and Verloo, M. G.: Water Extractability of Trace Metals from Soils: Some Pitfalls, Water. Air. Soil Pollut., 176, 21–35, https://doi.org/10.1007/s11270-005-9070-1, 2006.

Michaels, A. F., Bates, N. R., Buesseler, K. O., Carlson, C. A., and Knap, A. H.: Carbon-cycle imbalances in the Sargasso Sea, Nature, 372, 537–540, https://doi.org/10.1038/372537a0, 1994.

Nagata, T., Yamada, Y., and Fukuda, H.: Transparent Exopolymer Particles in Deep Oceans: Synthesis and Future Challenges, Gels, 7, 75, https://doi.org/10.3390/gels7030075, 2021.

Nosaka, Y., Yamashita, Y., and Suzuki, K.: Dynamics and Origin of Transparent Exopolymer Particles in the Oyashio Region of the Western Subarctic Pacific during the Spring Diatom Bloom, Front. Mar. Sci., 4, 2017.

Ortega-Retuerta, E., Passow, U., Duarte, C. M., and Reche, I.: Effects of ultraviolet B radiation on (not so) transparent exopolymer particles, Biogeosciences, 6, 3071–3080, https://doi.org/10.5194/bg-6-3071-2009, 2009a.

Ortega-Retuerta, E., Reche, I., Pulido-Villena, E., Agustí, S., and Duarte, C. M.: Uncoupled distributions of transparent exopolymer particles (TEP) and dissolved carbohydrates in the Southern Ocean, Mar. Chem., 115, 59–65, https://doi.org/10.1016/j.marchem.2009.06.004, 2009b.

Ortega-Retuerta, E., Mazuecos, I. P., Reche, I., Gasol, J. M., Álvarez-Salgado, X. A., Álvarez, M., Montero, M. F., and Arístegui, J.: Transparent exopolymer particle (TEP) distribution and in situ prokaryotic generation across the deep Mediterranean Sea and nearby North East Atlantic Ocean, Prog. Oceanogr., 173, 180–191, https://doi.org/10.1016/j.pocean.2019.03.002, 2019.

Pakulski, J. D. and Benner, R.: Abundance and distribution of carbohydrates in the ocean, Limnol. Oceanogr., 39, 930–940, https://doi.org/10.4319/lo.1994.39.4.0930, 1994.

Passow, U.: Formation of transparent exopolymer particles, TEP, from dissolved precursor material, Mar. Ecol. Prog. Ser., 192, 1–11, https://doi.org/10.3354/meps192001, 2000.

Passow, U.: Production of transparent exopolymer particles (TEP) by phyto- and bacterioplankton, Mar. Ecol. Prog. Ser., 236, 1–12, https://doi.org/10.3354/meps236001, 2002a.

Passow, U.: Transparent exopolymer particles (TEP) in aquatic environments, Prog. Oceanogr., 55, 287–333, https://doi.org/10.1016/S0079-6611(02)00138-6, 2002b.

867   Passow, U., Alldredge, A. L., and Logan, B. E.: The role of particulate carbohydrate exudates in the
868   flocculation of diatom blooms, Deep Sea Res. Part Oceanogr. Res. Pap., 41, 335–357,
869   https://doi.org/10.1016/0967-0637(94)90007-8, 1994.

870   Pilskaln, C. H., Villareal, T. A., Dennett, M., Darkangelo-Wood, C., and Meadows, G.: High concentrations
871   of marine snow and diatom algal mats in the North Pacific Subtropical Gyre: Implications for carbon and
872   nitrogen cycles in the oligotrophic ocean, Deep Sea Res. Part Oceanogr. Res. Pap., 52, 2315–2332,
873   https://doi.org/10.1016/j.dsr.2005.08.004, 2005.

874   van Pinxteren, M., Robinson, T.-B., Zeppenfeld, S., Gong, X., Bahlmann, E., Fomba, K. W., Triesch, N.,
875   Stratmann, F., Wurl, O., Engel, A., Wex, H., and Herrmann, H.: High number concentrations of
876   transparent exopolymer particles in ambient aerosol particles and cloud water – a case study at the
877   tropical Atlantic Ocean, Atmospheric Chem. Phys., 22, 5725–5742, https://doi.org/10.5194/acp-22-
878   5725-2022, 2022.

879   Prairie, J. C., Montgomery, Q. W., Proctor, K. W., and Ghiorso, K. S.: Effects of Phytoplankton Growth
880   Phase on Settling Properties of Marine Aggregates, J. Mar. Sci. Eng., 7, 265,
881   https://doi.org/10.3390/jmse7080265, 2019.

882   Quay, P., Emerson, S., and Palevsky, H.: Regional Pattern of the Ocean's Biological Pump Based on
883   Geochemical Observations, Geophys. Res. Lett., 47, e2020GL088098,
884   https://doi.org/10.1029/2020GL088098, 2020.

885   Quay, P., & Stephens, M. (2025). Regional patterns of organic matter export rates along the GEOTRACES
886   Pacific meridional transect GP15. *Global Biogeochemical Cycles*, *39*(2), e2024GB008277.

887   Quigg, A., Santschi, P. H., Burd, A., Chin, W. C., Kamalanathan, M., Xu, C., & Ziervogel, K. (2021). From
888   nano-gels to marine snow: A synthesis of gel formation processes and modeling efforts involved with
889   particle flux in the ocean. *Gels*, *7*(3), 114.

890   Rabouille, S., Cabral, G. S., and Pedrotti, M. L.: Towards a carbon budget of the diazotrophic
891   cyanobacterium Crocosphaera: effect of irradiance, Mar. Ecol. Prog. Ser., 570, 29–40,
892   https://doi.org/10.3354/meps12087, 2017.

893   Radić, T., Ivančić, I., Fuks, D., and Radić, J.: Marine bacterioplankton production of polysaccharidic and
894   proteinaceous particles under different nutrient regimes, FEMS Microbiol. Ecol., 58, 333–342,
895   https://doi.org/10.1111/j.1574-6941.2006.00176.x, 2006.

896   Reygondeau, G., Longhurst, A., Martinez, E., Beaugrand, G., Antoine, D., and Maury, O.: Dynamic
897   biogeochemical provinces in the global ocean, Glob. Biogeochem. Cycles, 27, 1046–1058,
898   https://doi.org/10.1002/gbc.20089, 2013.

899   Rochelle-Newall, E. J., Mari, X., and Pringault, O.: Sticking properties of transparent exopolymeric
900   particles (TEP) during aging and biodegradation, J. Plankton Res., 32, 1433–1442,
901   https://doi.org/10.1093/plankt/fbq060, 2010.

902   Roshan, S. and DeVries, T.: Efficient dissolved organic carbon production and export in the oligotrophic
903   ocean, Nat. Commun., 8, 2036, https://doi.org/10.1038/s41467-017-02227-3, 2017.

Sambrotto, R. N., Savidge, G., Robinson, C., Boyd, P., Takahashi, T., Karl, D. M., Langdon, C., Chipman, D., Marra, J., and Codispoti, L.: Elevated consumption of carbon relative to nitrogen in the surface ocean, Nature, 363, 248–250, https://doi.org/10.1038/363248a0, 1993.

Smith, D. C., Simon, M., Alldredge, A. L., and Azam, F.: Intense hydrolytic enzyme activity on marine aggregates and implications for rapid particle dissolution, Nature, 359, 139–142, https://doi.org/10.1038/359139a0, 1992.

Smyth, A. J., and Letscher, R. T.: Spatial and temporal occurrence of preformed nitrate anomalies in the subtropical North Pacific and North Atlantic oceans, *Marine Chemistry*, *252*, 104248, https://doi.org/10.5194/bg-15-6461-2018, 2023.

Sun, C.-C., Sperling, M., and Engel, A.: Effect of wind speed on the size distribution of gel particles in the sea surface microlayer: insights from a wind–wave channel experiment, Biogeosciences, 15, 3577–3589, https://doi.org/10.5194/bg-15-3577-2018, 2018.

Teng, Y.-C., Primeau, F. W., Moore, J. K., Lomas, M. W., and Martiny, A. C.: Global-scale variations of the ratios of carbon to phosphorus in exported marine organic matter, Nat. Geosci., 7, 895–898, https://doi.org/10.1038/ngeo2303, 2014.

Thompson, A. W., van den Engh, G., Ahlgren, N. A., Kouba, K., Ward, S., Wilson, S. T., and Karl, D. M.: Dynamics of Prochlorococcus Diversity and Photoacclimation During Short-Term Shifts in Water Column Stratification at Station ALOHA, Front. Mar. Sci., 5, 2018.

Thornton, D. C. O.: Coomassie Stainable Particles (CSP): Protein Containing Exopolymer Particles in the Ocean, Front. Mar. Sci., 5, 2018.

Toggweiler, J. R.: Carbon overconsumption, Nature, 363, 210–211, https://doi.org/10.1038/363210a0, 1993.

Verdugo, P.: Marine microgels, Annual Review of Marine Science, 4(1), 375-400, 2012.

Verdugo, P., Alldredge, A. L., Azam, F., Kirchman, D. L., Passow, U., & Santschi, P. H.: The oceanic gel phase: a bridge in the DOM–POM continuum. Marine chemistry, 92(1-4), 67-85, 2004.

Villareal, T. A., Pilskaln, C. H., Montoya, J. P., and Dennett, M.: Upward nitrate transport by phytoplankton in oceanic waters: balancing nutrient budgets in oligotrophic seas, PeerJ, 2, e302, https://doi.org/10.7717/peerj.302, 2014.

Westberry, T. K., Silsbe, G. M., and Behrenfeld, M. J.: Gross and net primary production in the global ocean: An ocean color remote sensing perspective, Earth-Sci. Rev., 237, 104322, https://doi.org/10.1016/j.earscirev.2023.104322, 2023.

Williams, P. J. le B., Quay, P. D., Westberry, T. K., and Behrenfeld, M. J.: The Oligotrophic Ocean Is Autotrophic, Annu. Rev. Mar. Sci., 5, 535–549, https://doi.org/10.1146/annurev-marine-121211-172335, 2013.

Wurl, O., Wurl, E., Miller, L., Johnson, K., and Vagle, S.: Formation and global distribution of sea-surface microlayers, Biogeosciences, 8, 121–135, https://doi.org/10.5194/bg-8-121-2011, 2011a.

940   Wurl, O., Miller, L., and Vagle, S.: Production and fate of transparent exopolymer particles in the ocean,
941   J. Geophys. Res. Oceans, 116, https://doi.org/10.1029/2011JC007342, 2011b.

942   Zamanillo, M., Ortega-Retuerta, E., Nunes, S., Estrada, M., Sala, M. M., Royer, S.-J., López-Sandoval, D.
943   C., Emelianov, M., Vaqué, D., Marrasé, C., and Simó, R.: Distribution of transparent exopolymer particles
944   (TEP) in distinct regions of the Southern Ocean, Sci. Total Environ., 691, 736–748,
945   https://doi.org/10.1016/j.scitotenv.2019.06.524, 2019.

946   Zamanillo, M., Ortega-Retuerta, E., Cisternas-Novoa, C., Marrasé, C., Pelejero, C., Pascual, J., Gasol, J. M.,
947   Engel, A., and Simó, R.: Uncoupled seasonal variability of transparent exopolymer and Coomassie
948   stainable particles in coastal Mediterranean waters: Insights into sources and driving mechanisms, Elem.
949   Sci. Anthr., 9, 00165, https://doi.org/10.1525/elementa.2020.00165, 2021.

950   Zäncker, B., Bracher, A., Röttgers, R., and Engel, A.: Variations of the Organic Matter Composition in the
951   Sea Surface Microlayer: A Comparison between Open Ocean, Coastal, and Upwelling Sites Off the
952   Peruvian Coast, Front. Microbiol., 8, 2017.

953

954